Climate Change and Emissions Impacts on Atmospheric PAH Transport to the Arctic

Citation: Friedman, Carey L., Yanxu Zhang, and Noelle E. Selin. "Climate Change and Emissions Impacts on Atmospheric PAH Transport to the Arctic." Environ. Sci. Technol. 48, no. 1 (January 7, 2014): 429–437.

As Published: http://dx.doi.org/10.1021/es403098w

Publisher: American Chemical Society (ACS)

Persistent URL: http://hdl.handle.net/1721.1/94640

Version: Author's final manuscript: final author's manuscript post peer review, without publisher's formatting or copy editing

Climate change and emissions impacts on atmospheric PAH transport to the Arctic

Carey L. Friedman[1*], Yanxu Zhang[2] and Noelle E. Selin[3]

[1][Center for Global Change Science, Massachusetts Institute of Technology, Cambridge, Massachusetts]

[2][School of Engineering and Applied Sciences, Harvard University, Cambridge, Massachusetts]

[3][Engineering Systems Division and Department of Earth, Atmospheric, and Planetary Science, Massachusetts Institute of Technology, Cambridge, Massachusetts]

*Correspondence to: C. L. Friedman (clf@mit.edu)

TOC Art

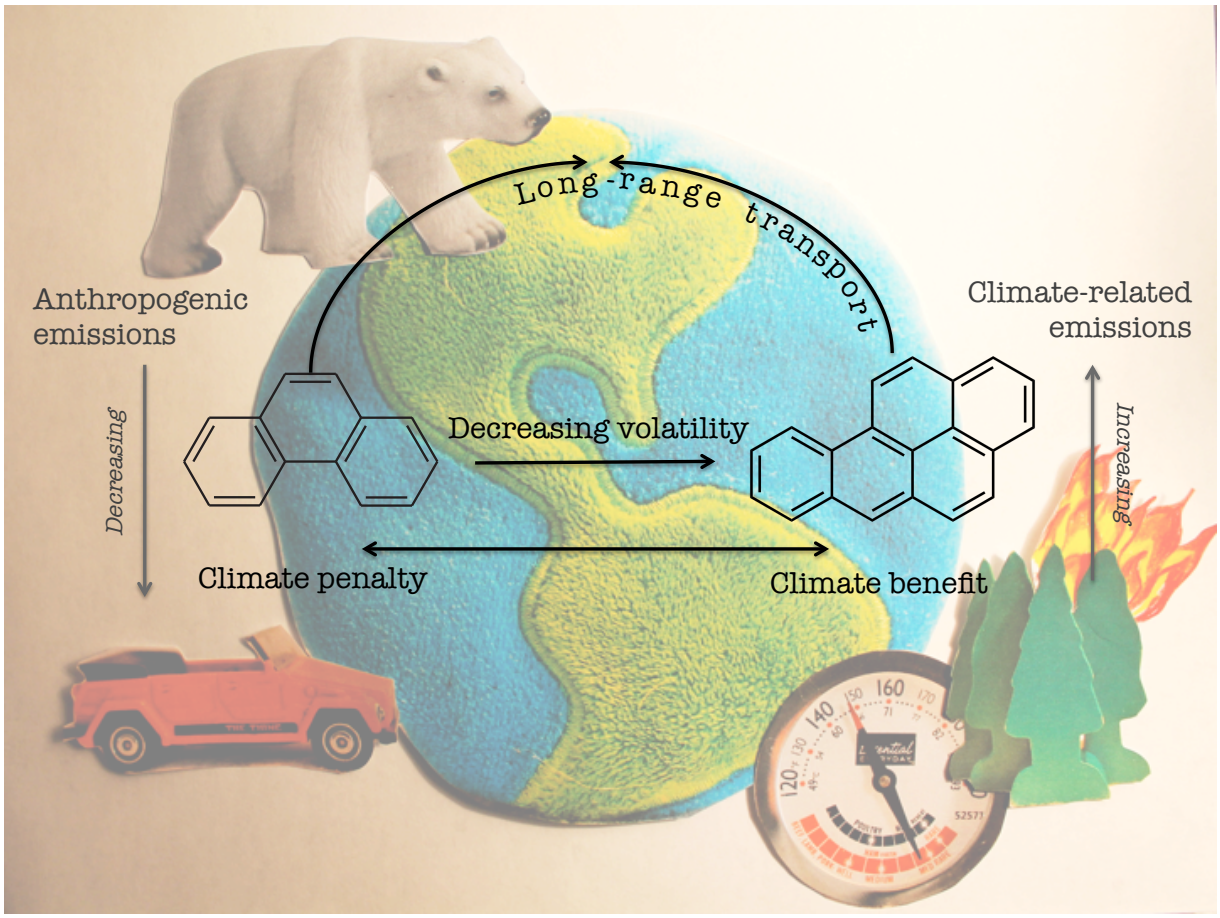

ABSTRACT

We investigate effects of 2000-2050 emissions and climate changes on the atmospheric transport of three polycyclic aromatic hydrocarbons (PAHs): phenanthrene (PHE), pyrene (PYR), and benzo[a]pyrene (BaP). We use the GEOS-Chem model coupled to meteorology from a general circulation model, and focus on impacts to northern hemisphere mid-latitudes and the Arctic. We project declines in anthropogenic emissions (up to 20%) and concentrations (up to 37%), with particle-bound PAHs declining more, and greater declines in mid-latitudes versus the Arctic. Climate change causes relatively minor increases in mid-latitude concentrations for the more volatile PHE and PYR (up to 4%) and decreases (3%) for particle-bound BaP. In the Arctic, all PAHs decline slightly under future climate (up to 2%). Overall, we observe a small 2050 "climate penalty" for volatile PAHs and "climate benefit" for particle-bound PAHs. The degree of penalty or benefit depends on competition between deposition and surface-to-air fluxes of previously-deposited PAHs. Particles and temperature have greater impacts on future transport than oxidants, with particle changes alone accounting for 15% of BaP decline under 2050 emissions. Higher temperatures drive increasing surface-to-air fluxes that cause PHE and PYR climate penalties. Simulations suggest ratios of more-to-less volatile species can be used to diagnose signals of climate versus emissions, and that these signals are best observed in the Arctic.

INTRODUCTION

Polycyclic aromatic hydrocarbons (PAHs), toxic compounds produced by the incomplete combustion of organic material, can travel long distances in the atmosphere. As such, PAHs are included in the Convention for Long-Range Transboundary Air Pollution's (CLRTAP's) Persistent Organic Pollutants (POP) protocol[1]. Recently, PAHs have been classified as "emerging contaminants in the Arctic" because body burdens in lower Arctic marine trophic levels are increasing while those of other POPs are declining[2]. Atmospheric transport is the most efficient way for PAHs released in the lower latitudes to reach the Arctic, and previous studies suggest long-range transport accounts for the majority of PAHs observed in Arctic air, especially in winter[3-7]. As conditions in the Arctic become favorable for activities causing local PAH emissions (e.g., transit and/or oil/gas shipping and related accidents/spills, wildfires, domestic combustion)[8-10], and climate changes could lead to alterations in transport and revolatilization[11-13], it is important to examine the changing influence of long-range

transport contributions to Arctic PAH levels. Documenting changes in atmospheric PAH concentrations can provide information to help further analyses of PAH exposure attribute Arctic burdens to specific sources.

PAHs are different from many other POPs in that they are byproducts of combustion (i.e., they are not intentionally produced) and their emissions are on-going. Emissions of most POPs have been extensively controlled in past decades; thus, most previous studies investigating impacts of future conditions on POP transport have looked primarily at climate changes, and not at anthropogenic activities affecting emissions. Lamon et al.[11] examined the multimedia behavior of PCBs under future climate and found increased PCB volatilization and atmospheric transport driven mostly by rising temperatures. Ma and Cao[12] developed an air-surface perturbation model to examine climate change effects on PCBs and pesticides, also finding higher temperatures increase air concentrations. Ma et al.[13] compared Arctic concentrations with simulations of the effect of climate change, finding that a wide range of POPs have already been remobilized in the Arctic because of sea-ice retreat and warming temperatures. Gouin et al.[14] review these and other studies and conclude that climate change will affect POP exposures within a factor of two. Wöhrnschimmel et al.[15] examined the effects of changing climate and emissions patterns on the distribution of hypothetical POP-like chemicals in the Arctic, finding increases of varying degrees depending on whether emissions were on-going or phased-out. Collectively, these studies suggest climate change increases air concentrations primarily because higher temperatures induce volatilization from other environmental media. This represents potential for increased transport to remote regions, and suggests global efforts to reduce POPs in the environment may be undermined by climate change[13].

The relative importance of climate versus emissions changes to atmospheric concentrations, however, has not been examined for existing POPs with on-going emissions. Previous work has investigated the influence of climate versus emissions for atmospheric constituents that simultaneously force climate and degrade air quality, such as ozone (O_3) and particulate matter (PM). Wu et al.[16] examined the influence of 2050 climate and anthropogenic emissions on global O_3, finding that 2050 anthropogenic emissions of O_3 precursors will increase the tropospheric O_3 burden by 17%, while climate-related changes lead to only a 1.6% increase. Pye et al.[17] evaluated the influence of 2050 climate and anthropogenic emissions on inorganic aerosol concentrations, finding considerable increases in global burdens of sulfate, nitrate, and

ammonium aerosols under 2050 anthropogenic emissions, but either no change or decreases in burdens under 2050 climate. Thus, it has generally been found that emissions reductions or increases dominate changes from climate to 2050; however, emissions impacts are highly uncertain, given the range of assumptions about growth and abatement measures[18].

Here, we evaluate 2000-2050 changes driven by future climate ("FC") and future emissions ("FE") separately, and together ("FCFE"), on atmospheric PAHs using the chemical transport model GEOS-Chem, with emphasis on transport to the Arctic and concentration changes. We compare emissions, concentrations, deposition, and oxidation globally, in the northern hemisphere (NH) mid-latitudes, and in the Arctic to a control simulation of present-day climate and emissions. We also evaluate the impact on PAHs of increased Arctic Ocean oil/gas exploration and transit shipping by including emissions estimates from future shipping in the FCFE scenario. Finally, we explore measurement constraints necessary for resolving anthropogenic versus climate influences on atmospheric PAH observations. Simulations are conducted for phenanthrene (PHE), pyrene (PYR), and benzo[a]pyrene (BaP) to capture a range of volatilities (PHE exists primarily in the gas phase, BaP is mostly particle-bound, and PYR partitions between both phases). We show that while climate change can induce both increases and decreases in atmospheric concentrations, depending on PAH volatility, these changes are minor compared to declines expected from lower anthropogenic emissions.

METHODS

Model description

We use the chemical transport model GEOS-Chem[19] (http://www.geos-chem.org/) to (1) simulate global atmospheric PAH transport in both the present and future (version 8-03-02) and (2) generate present and future concentrations of species interacting with PAHs (i.e., OC, BC, O_3, and OH) with a NO_x-Ox-hydrocarbon-aerosol simulation (version 9-01-02). Given substantially lower atmospheric PAH concentrations compared to aerosols and oxidants, and the computational intensity of the NO_x-Ox-hydrocarbon-aerosol simulation, we assume PAHs have a negligible impact on aerosols and oxidants and run the PAH and NO_x-Ox-hydrocarbon-aerosol models separately, with monthly mean aerosol/oxidant concentrations archived and used as input to PAH simulations. Sensitivity simulations suggest using daily rather than monthly oxidant and aerosol averages cause ≤2% differences in PAH concentrations (Fig. S1; Table S1 in the Supporting Information (SI)). Though there is

evidence secondary organic aerosol (SOA) affects atmospheric PAH transport[20] and that it accounts for a substantial (>30%) fraction of total organic matter[21], analyses of SOA influence on PAH transport suggest it has minimal impact because of the more dominant role of BC versus organic matter in partitioning[22]. The PAH simulation development and evaluation was recently detailed in full elsewhere[5], and we describe additional updates and reevaluation in SI. We use a global primary emissions inventory from 2004 compiled on a country-by-country basis for present-day[23], with emissions spatially allocated according to population (except for wildfires; see below) on a 1°×1° grid. The projection of future emissions, and meteorology used for both present and future simulations, are described below and in the SI. The NO_x-Ox-hydrocarbon-aerosol simulation has also been described extensively elsewhere[19, 24], and we provide a summary of the conditions used here in the SI.

PAH model updates The current model features updates relative to the previous version[5], which included gas-phase oxidation by OH (scaled for diurnal variation), gas-particle partitioning with OC and BC following the Dachs and Eisenreich scheme[25], and wet and dry deposition of gases and particles, with equilibrium assumed at each time step. Updates include incorporation of temperature-dependent gas-particle partitioning into the standard simulation, particle-phase PAH oxidation by O_3, and interannual variability in OC, BC, O_3, and OH with concentrations specific to each climate/emissions scenario. Additionally, particles with which PAHs are associated convert from hydrophobic to hydrophilic species with a lifetime of 1.2 days, following a scheme implemented for OC and BC aerosols within GEOS-Chem[24]. This conversion increases the efficiency of wet scavenging over time, with no change in PAH chemistry.

We include two improvements to PAH emissions. First, we alter the primary inventory by redistributing wildfire emissions within the source regions described below, following burned area spatial distribution in the Global Fire Emissions Database (GFED3; http://www.globalfiredata.org). Second, we incorporate re-emissions (i.e., gas-phase diffusive volatilization of previously-deposited PAHs) by introducing a level-III fugacity model[26-28] of soil-air and vegetation-air exchange. Re-emissions are sensitive to changes in temperature and atmospheric concentrations. Oceanic re-emissions are not considered as there is no clear indication of PAH out-gassing[29-31], nor from snow/ice surfaces due to lack of data. Though there is evidence of seasonal fluxes from lakes and coastal waters[32-34], we do not account for them, as the meteorology does not distinguish between solid land surfaces and freshwater.

Based on limited data[32-34], this likely neglects only small fluxes of volatile PAHs in late summer/early fall. Long-range PAH transport is more likely impeded by net absorption by lakes, which also likely has a minimal effect given that surface area and sorption capacity of lakes is small compared to soils, especially those rich in OC.

Meteorology All simulations are driven by output from the NASA Goddard Institute for Space Studies (GISS) general circulation model (GCM), resolved at 3 or 6 hours temporally, 4° latitude x 5° longitude, and 23 levels vertically. For present-day (representing 2000), we use the mean of 1997-2003; for the future (representing 2050), we use the mean of 2047-2053 generated under an SRES A1B scenario; these ranges are sufficient for capturing differences in climate[17, 35].

Methodology detail in SI PAH model details are reported in SI, including evaluations of model concentration and deposition results against those from its previous publication[5] and observations (Figs. S2-S4), development of the re-emissions model, comparisons of simulated re-emissions fluxes and fugacity gradients to observations (Table S2), and physicochemical constants (Table S3). In general, the updated model captures observed monthly mean concentrations and variation with similar or better skill compared to previously published results[5], while deposition biases high in both versions. Mean PHE, PYR, and BaP observed concentrations are simulated within factors of 1.6, 1.2, and 2.0 (mid-latitudes) and 1.1, 1.5, and 2.4 (Arctic), respectively. Summer Arctic simulated concentrations can be orders of magnitude lower than observed, likely due to local sources not considered within the model[36]. Deposition rates are simulated within factors of 2.4, 2.6, and 3.4. Though observations are limited, the re-emissions model predicts net surface-to-air fluxes mostly within the range of observations, and captures reported seasonal variations of fugacity ratios (largest ratios in June followed by September and November).

Future anthropogenic PAH emissions (FE scenario)

We scale present-day emissions to 2050 for five source regions having potential impacts on the Arctic. Four of the regions are those designated by the Task Force on Hemispheric Transport of Air Pollution (TF HTAP; http://www.htap.org): (Europe: 10W–50E, 25N–65N; North America: 125W–60W, 15N–55N; East Asia: 95E–160E, 15N–50N; South Asia: 50E–95E, 5N–35N). We also scale emissions from Russia (50E–180E, 50N–75N) given their influence on European Arctic concentrations[3, 5].

For each source region, we scale PHE, PYR, and BaP emissions from activities contributing substantially to global Σ16PAH emissions according to projected variables related to each activity. These activities include biomass burning, coke production, domestic coal combustion, and vehicle emissions. We aim to scale present-day emissions to 2050, though in some instances are limited by projections and scale to earlier years as risk-conservative estimates (noted below). For all scaling relying on International Energy Agency (IEA) projections, we use quantities estimated under the IEA's "New Policies Scenario", which assumes cautious global implementation of existing policy commitments[37]. For each PAH, we conduct a +/-20% emissions scaling sensitivity analysis, based on uncertainties in the present day inventory, to test the influence of uncertainty in future anthropogenic emissions on results.

Biomass burning Traditional biomass burning (the intentional burning of straw, firewood, and animal dung – not including wildfires) is a major source of energy in developing countries, but occurs to a lesser degree in developed countries, primarily in wood-burning stoves[38-40]. We scale biomass-burning emissions in East and South Asia according to the IEA's projections for biomass demand in developing countries. As incomes rise, demand is expected to decrease by 60% in China and ~6% in India between 2008 and 2035[41]. As conservative estimates for 2050, we scale emissions from the entire East and South Asian source regions by these factors, respectively. For all other regions, we do not expect biomass use to change substantially and do not scale emissions.

Coke production Global energy consumption in the iron and steel production sector from coking coal use is expected to double between 2000 and 2020 (from ~300 to 600 million tones of coal equivalent) and then decline until reaching ~180% of 2000 activity by 2035[37]. Due to lack of regional projections, we scale all source regions by 180% as risk-conservative estimates. Changes in emissions factors (EFs) may play a bigger role in future emissions than increase in coke demand, however. The present-day inventory assumes two types of coke ovens: beehive and large-scale[42]. Beehive ovens have a higher PAH EF than large-scale (490 versus 8 mg/kg, respectively), and the present-day inventory assumes percentage of coke produced by beehive ovens is 15% in China, 5% in India, 1% in Russia, and 0.1% in the U.S. and Europe[23]. These percentages will likely decrease substantially by 2050 in developing countries. Based on discussions elsewhere[42, 43], we assume that beehive oven use will decrease

by 2050 to 5% in East Asia, 1% in South Asia, 0.5% in Russia, and 0.05% in the U.S. and Europe, and scale emissions accordingly.

Domestic coal combustion Coal is an important source of cooking fuel and heat in developing countries, particularly in China due to rich reserves[23]. We consider domestic coal a traditional fuel source and scale emissions from its consumption as for biomass burning. Coal combustion for power generation is not considered, as it is a minor part of present-day emissions because of much lower EFs.

Vehicle emissions Shen et al.[44] applied EF prediction models to project 1971-2030 PAH emissions from vehicles based on gasoline and diesel consumption estimated under the IPCC A1B scenario. Here, we use Shen et al.'s 2030 estimates as proxies for 2050. These projections likely overestimate 2050 Asian emissions, as both India and China are projected to experience steep emissions declines starting ~2030. Though remaining source regions are also projected to experience declines through 2030, the rate of decline is considerably slower.

Arctic shipping We project emissions from oil/gas exploration ship activity and transit shipping (Fig. S5) following Peters et al.[8], who estimated 2050 emissions of climate-relevant atmospheric species from expanded Arctic Ocean petroleum and shipping. We calculate 2050 BaP emissions from Arctic shipping by multiplying Peters et al.'s estimates of 2050 oil/gas exploration and transit shipping BC emissions by a ratio of BaP and BC EFs. We use a BaP EF of 3.3×10^{-5} kg/tonne residual fuel oil for a crude tanker at sea[45], and a BC EF of 0.36 kg/tonne residual fuel oil[8]. We assume present-day Arctic shipping emissions are zero.

Particles and oxidants under FE A summary of the NO_x-Ox-hydrocarbon-aerosol simulation conditions used to generate aerosol and oxidant concentrations under FE is given in the SI, including assumptions regarding changes in emissions (Tables S4 and S5) and changes in surface concentrations (Figs. S6-S9 and Table S6). In general, surface-level OC and BC concentrations decrease, while O_3 and OH increase.

Future climate (FC scenario)

Meteorology GISS general circulation model data generated under the IPCC's A1B scenario is used to drive PAH transport in future climate. Global mean surface air and land temperatures both increase by 1.6 K, and precipitation increases 5%, with greatest increases in the intertropical convergence zone. Changes in boundary layer height and less frequent frontal

passages cause pollution to linger longer near source regions in the future[16, 17, 35], though there is also evidence of a strengthening and northward shift in mid-latitude westerlies, particularly in the fall[17]. Further discussion of differences in meteorological variables between future and present-day GCM output can be found elsewhere[16, 17, 35]

Wildfire emissions We scale PAH emissions in the FC scenario to reflect predicted future wildfire activity. The potential for wildfire and length of fire season are expected to increase in many regions from rising temperatures and less precipitation. Though projected changes are uncertain and strongly depend on climate model/emissions scenario, several studies generally agree on wildfire increases in the US, central/southern Europe, and central Asia[46-49]. As upper estimates, we scale emissions from the entire European, North American, and South Asian source regions according to one-half the most extreme increase in fire index predicted under future climate[46]:

$$WFI\ scale\ factor = \frac{WFI_{pres} + \max(\Delta WFI)/2}{WFI_{pres}}$$

where WFI_{pres} is present-day wildfire index and max(ΔWFI) is the maximum difference between future and present-day wildfire index in a given region. There is less agreement on future wildfires in East Asia and Russia. East Asian wildfire potential has been projected to increase, but not as greatly as in mid and south Asia[46-48]. Though increases in Siberian fire potential have been projected[9, 50, 51], when vegetation is held constant the increase is smaller because of less flammable resource[48]. This is important because changes in fire potential are expected to occur more rapidly than changes in vegetation[52]. Thus, as risk-conservative estimates, we increase emissions in East Asia by half the increase in South Asia, and in Russia by half the greatest predicted increase in annual dangerous fire days[51]. Sensitivities to these assumptions are discussed in the SI.

Particles and oxidants under FC A summary of NO_x-Ox-hydrocarbon-aerosol simulation conditions used to generate aerosol and oxidant concentrations under FC, including assumptions regarding changes in natural emissions, is in the SI. In general, the FC simulation produces slightly lower surface-level concentrations of all species compared to the control (Figs. S6-S9, Table S6).

RESULTS

Results are presented in the format of the model budget, starting first with PAH sources (emissions), then steady state concentrations, and finally sinks (deposition and oxidation).

Emissions

Each activity's contribution to present-day emissions within each source region is summarized in Tables S7 (anthropogenic) and S8 (climate-related). The contribution of individual activities to present-day emissions varies across regions, though not greatly between PAHs. For example, biomass burning dominates in Asia, while vehicle emissions are most important in North America. Wildfires contribute substantially to present-day emissions in North America and Russia, but matter less in other regions.

Under FE, decreases are observed in all but one region (BaP increases in Russia), with reductions greatest in East Asia and smallest in Russia. Factors for scaling anthropogenic emissions and subsequent changes in totals are presented in Table S7. Conversely, under FC, emissions increase in all regions except East Asia, from as little as 1% in Europe (PYR and BaP) to as much as 16% in North America (PYR).

As with regional, global emissions decrease under FE and increase under FC. Table S9 summarizes global primary, re-, and total emissions in the control, and changes under each future scenario. Under FE, BaP emissions decrease most, and PHE decreases least, while under FC, PHE emissions increase most and BaP least. The discrepancy can be attributed to differences in re-emissions. A substantial fraction (16%) of total PHE emissions are from re-emissions in the control, and this fraction increases (to 19%) under both FE and FC (under FE, because of lower atmospheric concentrations driving greater diffusive net fluxes from surface to air; under FC, because of higher temperatures). These increases offset declining primary emissions under FE and enhance increasing primary emissions under FC. By contrast, only 1% of BaP emissions are from re-emissions in the control and changes under FC and FE are negligible. Thus, changes in total BaP emissions predominantly reflect primary emissions changes. PYR emissions behave intermediate to PHE and BaP, and emissions in the FCFE scenario are nearly additive combinations of those under FE and FC.

We include projections of BaP emissions from transit and oil/gas exploration shipping in the Arctic in a sensitivity simulation of our FCFE scenario (Fig. S5). These emissions total only 1.6 Mg, or 0.05% of the global total under FCFE.

Though there is uncertainty in future emissions, predictions generally agree on declines for anthropogenic PAHs and co-emitted species[37, 41, 44, 53]. Sensitivity simulations suggest +/-20% changes to emissions projections result in, at most, corresponding NH concentration changes of +/-11%. Furthermore, a comparison between the relative uncertainties in emissions[23] and the range of physicochemical constants values reported in the literature (Table S10) suggests emissions uncertainties are likely a relatively minor contributor to present-day concentration uncertainties, though this is an area for further research. Thus, we consider projections of PAH emissions relative to one another to be robust.

Concentrations

Figures 1, S10, and S11 (panel A) show the global distributions of PHE, PYR, and BaP total atmospheric concentrations (gas + particulate) in the control, respectively. Panels B, C, and D show the difference in concentration between the FE, FC, and FCFE simulations and the control, respectively. Table S11 summarizes percent change in mean global, NH, mid-latitude (5-60°N), and Arctic (60-90°N) concentrations compared to the control. In the control, PHE has the highest concentrations and BaP the least, with highest concentrations closer to areas with high emissions like China and India.

Under FE, concentrations decrease for each PAH. BaP decreases most and PHE least, similar to emissions, and decreases are greatest in the mid-latitudes and least in the Arctic. There is also a shift from particles to the gas phase. The shift is greatest for BaP (gas phase increases 2%) because >50% of its mass is particulate (PYR and PHE have <5% and <1% in the particle phase). The shift is due primarily to fewer particles under FE. An FE sensitivity simulation demonstrates that there is no change in particulate/gas speciation when present-day particle concentrations are used. Declining particle concentrations also drive the decrease in total concentrations for particle-bound PAHs under FE: 15%, 10%, and <1% of the decrease in BaP, PYR, and PHE in the NH can be attributed to lower particle concentrations. Arctic concentrations decline less than mid-latitudes under FE. Ratios of Arctic to mid-latitude concentrations increase; i.e., PAHs are transported to the Arctic more efficiently. The increase in efficiency is greatest for BaP and least for PHE (+23%, +33%, and +47% for PHE, PYR,

and BaP, respectively). Some of this is due to lower particle concentrations. For example, a sensitivity simulation of FE with present-day particle concentrations shows BaP and PYR ratios increase less (+41% and +30%, respectively; PHE is not impacted). Overall, simulations suggest the Arctic responds slowly to mid-latitudes emissions reductions.

Under FC, only small changes in concentrations are observed and the direction of change depends on the PAH. PHE and PYR concentrations increase slightly everywhere (up to +5%) except over the Arctic, while BaP concentrations decrease slightly (up to -3%). Similar to FE, all PAHs shift to the gas phase, with BaP again showing the greatest shift (+3% in the gas phase). Gas-phase fractions increase primarily from rising temperatures and decreasing particle concentrations. Under FC, volatile PAHs transport to the Arctic less efficiently and particle-bound PAHs transport more efficiently (i.e., Arctic to mid-latitude concentration ratios change by -6%, -4%, and +2%, for PHE, PYR, and BaP, respectively).

As with emissions, concentrations under FCFE are nearly additive combinations of FE and FC. Thus, concentrations decline for all three PAHs, but PHE and PYR experience small "climate penalties", or offsets in the decreases from anthropogenic emissions due to increases in emissions associated with climate change. The climate penalty is 19% for PHE in the NH and 10% for PYR. Alternatively, BaP experiences a small "climate benefit", in which declining concentrations from anthropogenic emissions are further decreased because of climate changes. The BaP climate benefit is an additional decline of 5% of the anthropogenic decrease. Particle phase shifts are negligible for PHE, but the gas phase increases 2% and 5% for PYR and BaP, respectively. Including projected Arctic shipping emissions in the FCFE simulation diminishes BaP reductions observed without shipping. Thus, in the Arctic there is also a "future shipping penalty" of 21%, but globally and in the mid-latitudes, the impact is negligible. Though the magnitude of projected shipping emissions is uncertain due to a paucity of ship engine EF data and uncertainties in BC projections[8], our analysis suggests even moderate increases in Arctic emissions impact otherwise declining concentrations. Other Arctic emissions sources not accounted for here could have similar effects, such as increasing wildfire activity or domestic burning as the region becomes more populated[54, 55].

Uncertainties in simulated concentrations depend on uncertainties in emissions, PAH physicochemical constants, meteorological variables, and aerosol and oxidant concentrations. Sensitivity simulations conducted in a previous study[5] suggest oxidation rate uncertainties have large impacts on simulated concentrations, but the impact on 2000-2050 differences

should be relatively minor. Rather, uncertainties in the temperature dependence of partition coefficients and oxidation rate constants (Table S10) are likely to play larger roles in affecting 2000-2050 differences.

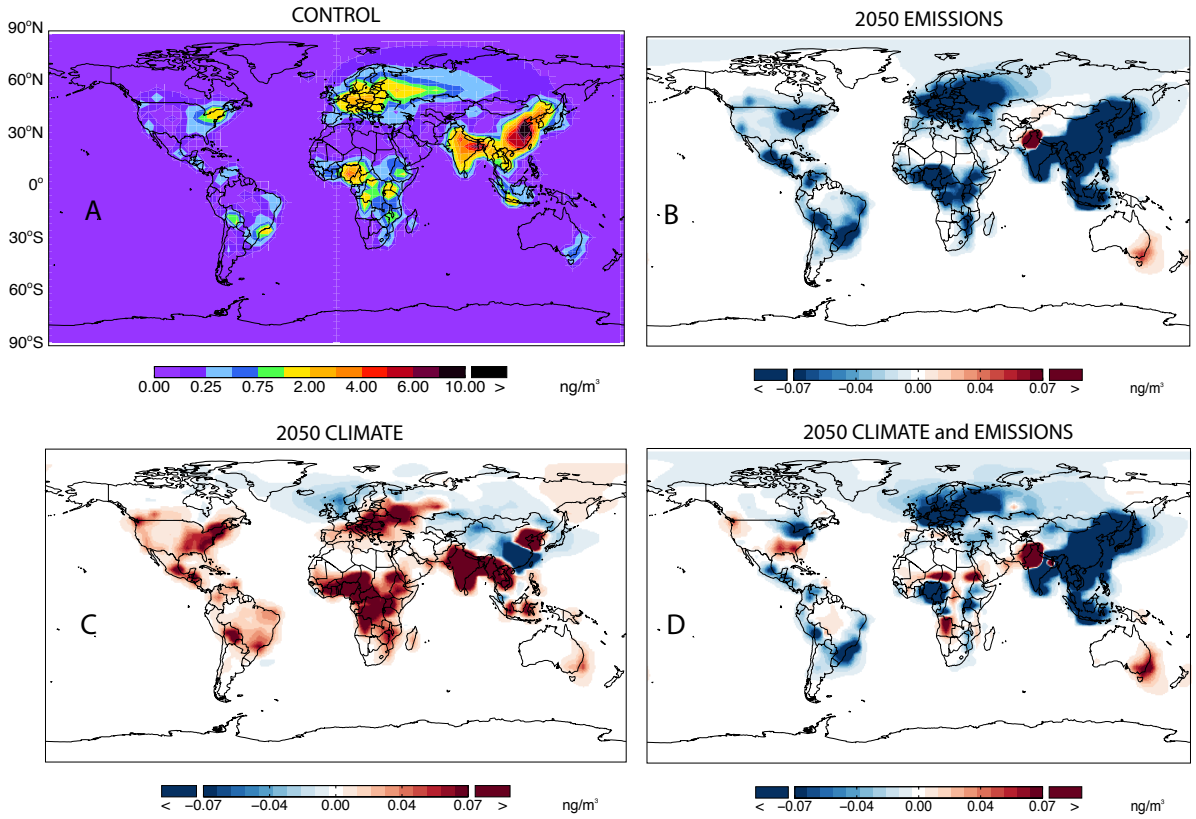

Figure 1. PHE concentrations under (A) the control; concentration differences between the control and simulations under (B) future emissions (FE); (C) future climate (FC), and; (D) future climate, future emissions (FCFE). Increases shown in red; decreases in blue.

Deposition

Table S12 summarizes annual global deposition in the control and changes in each future simulation. In the control, BaP has the greatest fraction of mass removed via deposition (30%), and PHE the least (9%). The contribution of gas versus particulate and wet versus dry to total deposition varies. Particulate wet and dry deposition and gaseous wet deposition are greatest for BaP and least for PHE. Gaseous dry deposition, however, removes the greatest fraction of PYR, followed by PHE and BaP. This is because PYR and PHE have similarly high gas-phase fractions compared to BaP, but gaseous dry deposition is dependent on the

octanol-air partition coefficient (K_{OA}), and the K_{OA} of PYR is >10x greater than that of PHE (Table S3).

Under FE, deposition decreases compared the control. All forms of PHE and PYR deposition decrease, with total deposition reductions of ~10%. Though declines in BaP particulate deposition drive a total deposition decrease of 10%, gas-phase BaP deposition increases (25% for dry, 15% for wet) because of the substantial shift to the gas phase.

Under FC, small total deposition increases (up to +3%) for each PAH are driven by increasing gas-phase dry deposition (up to +20%, for BaP), which is in turn again due to shifts from the particle to gas phase. All other forms of PHE and PYR deposition decline. Though gaseous BaP wet deposition also increases, it is only a small fraction of the total.

In the FCFE scenario, total PAH deposition decreases, though not by as much as under FE. Thus, we see a climate penalty in deposition for each PAH (up to 30%, for PYR). All forms of deposition decline for PHE and PYR, but there is a nearly 50% increase in gas-phase BaP dry deposition and a 25% increase in gaseous wet deposition because of the substantial shift to the gas phase. These large increases are outweighed by declines in particulate deposition, however.

Deposition is controlled primarily by the air-water partition coefficient (K_{AW}; for wet), and K_{OA} (for dry). Both of these constants have small uncertainty ranges compared to other physicochemical constants (such as k_{OH} or K_{BC}; Table S10). Thus, present-day deposition estimates are likely more robust than other simulated quantities, such as concentration or oxidation, but 2000-2050 changes in deposition may be relatively more sensitive to uncertainties because of the temperature dependence of K_{AW} and K_{OA}.

Oxidation

Table S13 summarizes annual global oxidation in the control and changes in each future scenario. Oxidation accounts for ~70-90% of atmospheric PAH removal in the control, with OH more important than O_3.

Under FE, gas-phase oxidation by OH increases for each PAH (up to +7%, for BaP). O_3 oxidation decreases for BaP (-4%) and there are negligible changes for PHE and PYR. Combined, the total oxidized fraction increases for each PAH. Changes in oxidation accelerate the decline of gas-phase PAHs. An FE sensitivity simulation with present-day

oxidants demonstrates that oxidation increases account for 8%, 10%, and 19% of the decline in NH BaP, PYR, and PHE concentrations, respectively. Increasing oxidation is the main reason for decreasing deposition under FE.

Under FC, BaP oxidation by OH increases (+2%) and by O_3 decreases (-3%), resulting in a 1% decline in total oxidation. There are only very small decreases in PHE and PYR oxidation (<1%). Oxidation does not strongly impact transfer from particles to gas, but does limit increasing concentrations of volatile PAHs. For example, even though mean surface-level OH and PHE oxidation decrease under FC, when present-day OH and O_3 concentrations are used in an FC sensitivity simulation, NH PHE concentrations increase by an additional 2%. Also, Arctic concentrations of PHE increase (+4%) rather than decrease, causing the Arctic to mid-latitude ratio to decline less (-2%). This is because regions where OH increases under FC (balanced by decreases elsewhere; Fig. S6) are also regions with high PAH emissions (e.g., China and Europe).

Under FCFE, total oxidation increases for each PAH (+2%, +2%, +3% for PHE, PYR, and BaP); this is driven by the increase in OH oxidation under FE.

Given either (1) very large uncertainties in oxidation rate constants because of difficultly with their empirical determination (e.g., k_{OH} for PYR and BaP are calculated from ionization potentials) or (2) oxidation being a major sink for primarily gas-phase PAHs (e.g., PHE), it is likely oxidation rate constant uncertainty contributes substantially to present-day simulated concentration uncertainty. Changes to oxidation in the future are relatively minor compared to changes in other metrics, however, and associated uncertainties remain the same across scenarios, so 2000-2050 differences in oxidation are likely relatively robust.

Using simulations to infer climate versus anthropogenic influences in measurements

We take advantage of the different behaviors of PHE and BaP to examine whether certain locations or seasons are sensitive to future emissions versus climate. We first look at mean annual change in simulated PHE/BaP under FE and FC in the NH (Fig. 2) and find that the Arctic, especially northwestern Canada and Alaska, is particularly sensitive to future scenarios, and that the direction of change is opposite for future climate versus emissions. In the control (panel A), the greatest values of PHE/BaP are generally in remote areas, such as in the Arctic, or over areas with low soil organic carbon content and high surface temperatures

(e.g., Chad and Niger) which cause large differences in re-emissions. For both FE and FC, the regions where the magnitude of PHE/BaP change is greatest is in similar locations, with FE showing PHE/BaP increases and FC showing declines. We then compare the mean annual simulated PHE/BaP to observed PHE/BaP (Fig. S12) over the entire Arctic (60-90N) and in the high Arctic (80-90N). The control simulates the measured ratio from the entire Arctic well, but the relatively small predicted changes from FE and FC are well within the large standard error of mean observed PHE/BaP. For the high Arctic, however, even though the control biases high compared to observations, predicted changes from FE and FC are greater than the standard error of the observed mean. Comparing observed ratios from the entire Arctic and high Arctic demonstrates that an increasing PHE/BaP value with latitude, as simulated in the control (from 21 to 156), is also detected in observations (from 23 to 80; Fig. S12). Neither FE nor FC substantially change PHE/BaP seasonal variation, and no single season clearly resolves the impact of future emissions versus climate.

Uncertainties associated with the FE and FC scenarios need to be considered when interpreting future PHE/BaP, especially under FE given its relatively greater uncertainty. Given differences in PHE and BaP's spatial emissions distributions and non-linear removal by oxidation, we examine how the FE PHE/BaP ratio is affected when factors for scaling emissions are augmented by +/-20% for both PHE and BaP. Though high Arctic concentrations only change by +/-8% (PHE) and +/-10% (BaP), the FE ratio can range from -17% to +20%, or from slightly less than the control ratio to 1.4x the control (Fig. S12). The range in the ratio is much smaller when the augmentation is in the same direction for both PAHs; e.g., when both PHE and BaP emissions are reduced by 20%, PHE/BaP changes by only -2%. Thus, the conclusion that PHE/BaP increases under FE is more robust when PHE and BaP emissions decline at similar rates. Observed long-term trends indicate that PHE/BaP in the high Arctic is indeed increasing[7].

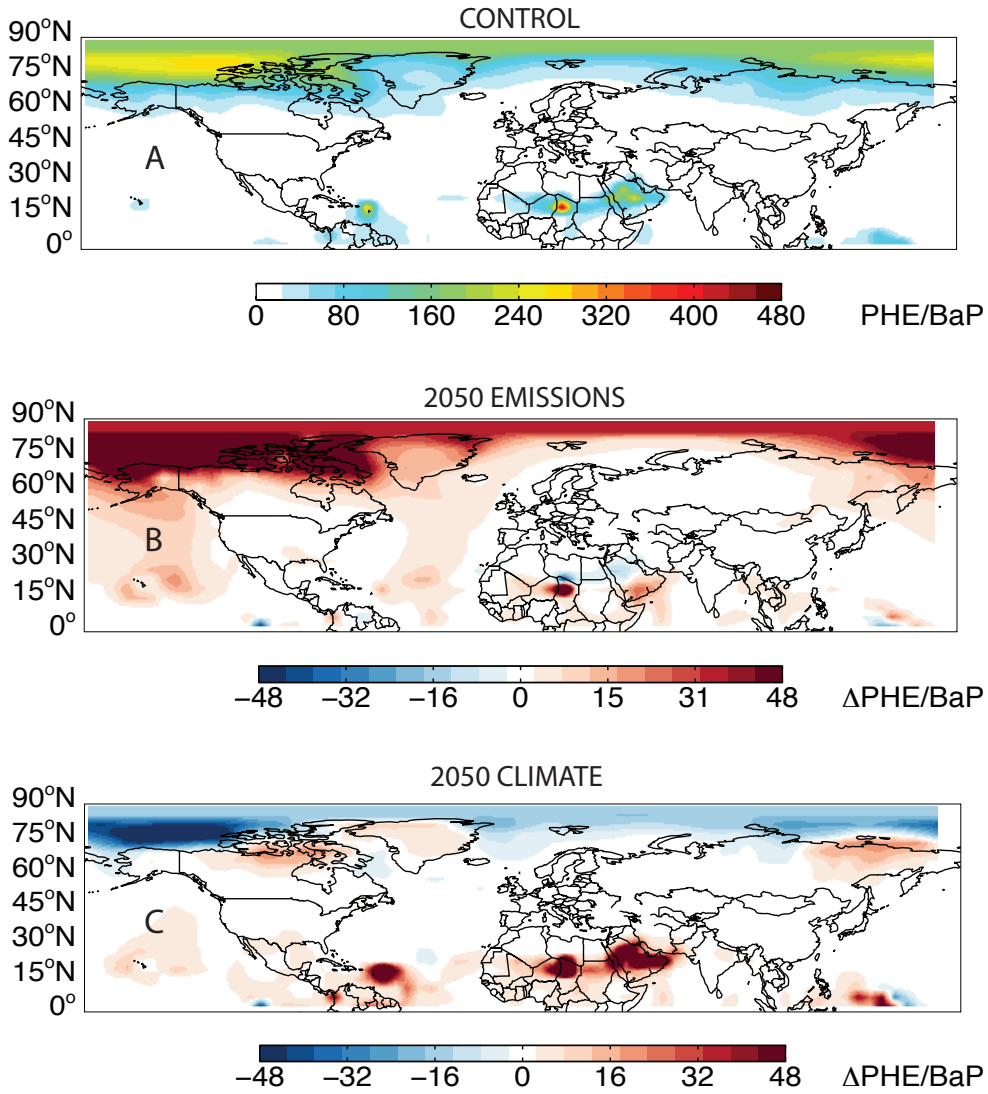

Figure 2. Mean annual northern hemisphere [PHE]/[BaP] in the control (A) and the deviation of this ratio under (B) future emissions (FE), and (C) future climate (FC). Red marks increases; blue marks decreases.

DISCUSSION

2000 to 2050 changes in simulated atmospheric PAH concentrations are driven by declining anthropogenic emissions, with declining concentrations predicted for each PAH simulated. Concentration decreases are more substantial for particle-bound PAHs. This is because PAHs respond differently to climate change depending on their volatility, with behavior under future climate controlled primarily by competition between increasing deposition and increasing re-emissions. Volatile PAH concentrations increase in response to climate change because re-

emissions increases outweigh deposition increases, while the opposite is true for particle-bound PAHs. Thus, we observe small "climate penalties" for volatile PAHs (PHE and PYR), and a small "climate benefit" for particle-bound PAHs (BaP).

As mentioned above, though there are substantial uncertainties in emissions projections, quantitative uncertainty analyses suggest emissions play a relatively minor role in simulated present-day concentration uncertainty compared to physicochemical constants[56]. 2000-2050 deposition and re-emissions changes that drive diverging behaviors under future climate are controlled mostly by particle concentrations and the magnitude and temperature-dependence of partition coefficients. This suggests that physicochemical parameters governing these processes (i.e., K_{OA}, K_{BC}, and enthalpies of phase transfer) will have the greatest impacts on whether climate change enhances or offsets declining concentrations from lower emissions. Though oxidation plays a relatively minor role in 2000-2050 concentration changes, there are substantial uncertainties in oxidation reaction rate constants compared to other physicochemical parameters[56], suggesting greater uncertainty associated with projections of PAHs that are more susceptible to loss via oxidation (e.g., PHE). Thus, while we have confidence that anthropogenic emissions will decline and that PAHs with different volatilities will behave differently in response to climate, the absolute magnitude of the impact on concentrations is less certain, as is the degree to which volatility-dependent behaviors will diverge.

Changes in the simulated PHE/BaP ratio suggest the high Arctic is a priority area for observations aimed at resolving the influence of changing climate versus anthropogenic activities. The fact that the simulated control PHE/BaP ratio in the high Arctic biases high compared to observations should be considered alongside this finding, however. On the model side, annual Arctic PHE concentrations are systematically overestimated and BaP concentrations are underestimated. Uncertainties in measurements may also play a role. Long sampling times required to accumulate detectable masses in the Arctic can lead to known low biases in volatile PAHs (e.g., PHE), while concentrations of low-volatility PAHs (e.g., BaP) are often below analytical limits of quantification (LOQs) (Hayley Hung, personal communication). A common practice for reporting concentrations below LOQs is to estimate true values with a fraction of the LOQ, and this can lead to high biases in lower-volatility PAHs. These factors, combined with the model's ability to simulate concentrations orders of magnitude below LOQs, help explain some of the difference between the control and

observed PHE/BaP. Despite this discrepancy, and analytical and practical obstacles associated with measuring PAHs in the high Arctic, our results emphasize the importance of improving long-term measurements within this region. The continued monitoring of PAHs in particular is in accord with the TF HTAP's recommendation that mitigation strategies focus on POPs co-emitted with other combustion byproducts because of potential co-benefits[57].

There are additional uncertainties in our simulations not yet discussed, including but not limited to the parameterization of gas-particle partitioning (e.g., we do not address SOA here), projections of future oxidants and particles, and the influence of other potentially important oxidants (e.g., NO_3). Another substantial uncertainty is how surface-atmosphere exchange will evolve in future climate. In our model, atmospheric PAHs do not interact with surface water, snow, or ice, and results are likely strongly dependent on surface cover parameterizations. Explicitly including these substances and surface-atmosphere exchange could result in considerable differences in Arctic concentrations and thus in our estimates of Arctic PHE/BaP. Ice and snow cover can be efficient scavengers of atmospheric PAHs[58], and as such, reduced ice/snow cover could weaken an important atmospheric removal process. Melting ice opens the possibility for air-water exchange and uptake of PAHs into the ocean[59], and air-water exchange is in turn influenced by changing concentrations of phytoplankton and oceanic OC[60]. At present, little is known about PAH exchange between the atmosphere and Arctic surface environments. Identifying key processes and rates should be a priority for future research, especially given the recent discovery that PAHs dominate the POP body burden of Arctic marine invertebrates and fish[2], suggesting a complex relationship between the ocean and atmosphere.

We also note that while we assess climate penalties and benefits with respect to atmospheric concentrations, we do not examine the fate of PAHs within other environmental media. It is possible that an atmospheric climate benefit could simultaneously be a lake or soil climate penalty. In addition, given that the greatest increases due to climate changes are no more than +5% of present day concentrations, it is possible that further studies employing multimedia or ecosystem models may find no basis for concern regarding potential increases in exposures.

Finally, our results should be interpreted within the context of model evaluation against observations. Nearly all of the changes observed under 2050 scenarios are within the range of model-measurement discrepancies (see Figs. S2-S4), as well as the range of uncertainty in PAH measurements.

Supporting Information

The supporting information includes model evaluations, a description of the re-emissions model, and tables and figures summarizing primary and re-emissions, concentrations (PAH, particles, and oxidants), deposition, oxidation, and Arctic PHE/BaP results. This information is available free of charge via the internet at http://pubs.acs.org/.

Acknowledgements

Funding was provided by NSF Atmospheric Chemistry (#1053658), Arctic Natural Sciences (#1203526), and Dynamics of Coupled Natural and Human Systems (#1313755) Programs, and MIT's Leading Technology and Policy Initiative. We thank Glen Peters and Stig Dalsøren (CICERO) for Arctic shipping emissions data, Xu Yue and Bess Corbitt (Harvard University) for discussions surrounding wildfires and providing soil carbon data, respectively, Colin Pike-Thackray (MIT) for physicochemical constant value ranges, and Eric Leibensperger (SUNY Plattsburgh) and Shiliang Wu (MTU) for assistance with GCM data.

References

1. UNECE *Protocol to the 1979 Convention on Long-Range Transboundary Air Pollution on Persistent Organic Pollutants*; United Nations Economic Commission for Europe: Aarhus, DM, 1998.

2. De Laender, F.; Hammer, J.; Hendriks, A. J.; Soetaert, K.; Janssen, C. R. Combining monitoring data and modeling identifies PAHs as emerging contaminants in the Arctic. *Environ. Sci. Technol.* **2011,** *45*, 9024-9029.

3. Halsall, C. J.; Barrie, L. A.; Fellin, P.; Muir, D. G. C.; Billeck, B. N.; Lockhart, L.; Rovinsky, F.; Kononov, E.; Pastukhov, B. Spatial and temporal variation of polycyclic aromatic hydrocarbons in the Arctic atmosphere. *Environ. Sci. Technol.* **1997,** *31*, 3593-3599.

4. Halsall, C. J.; Sweetman, A. J.; Barrie, L. A.; Jones, K. C. Modelling the behaviour of PAHs during atmospheric transport from the UK to the Arctic. *Atmos. Environ.* **2001,** *35*, 255-267.

5. Friedman, C. L.; Selin, N. E. Long-range atmospheric transport of polycyclic aromatic hydrocarbons: A global 3-D model analysis including evaluation of Arctic sources. *Environ. Sci. Technol.* **2012,** *46*, 9501-9510.

6. Wang, R.; Tao, S.; Wang, B.; Yang, Y.; Lang, C.; Zhang, Y.; Hu, J.; Ma, J.; Hung, H. Sources and pathways of polycyclic aromatic hydrocarbons transported to Alert, the Candian High Arctic. *Environ. Sci. Technol.* **2010,** *44*, 1017-1022.

7. Becker, S.; Halsall, C. J.; Tych, W.; Hung, H.; Attewell, S.; Blanchard, P.; Li, H.; Fellin, P.; Stern, G.; Billeck, B.; Friesen, S. Resolving the long-term trends of polycyclic aromatic hydrocarbons in the Canadian Arctic atmosphere. *Environ. Sci. Technol.* **2006,** *40*, (10), 3217-3222.

8. Peters, G. P.; Nilssen, T. B.; Lindholt, L.; Eide, M. S.; Glomsrød, S.; Eide, L. I.; Fuglestvedt, J. S. Future emissions from shipping and petroleum activities in the Arctic. *Atmos. Chem. Phys.* **2011,** *11*, 5305-5320.

9. Flannigan, M. D.; Stocks, B.; Turetsky, M.; Wotton, M. Impacts of climate change on fire activity and fire management in the circumboreal forest. *Glob. Change Biol.* **2009,** *15*, 549-560.

10. WWF *Oil Spill Response Challenges in Arctic Waters*; Oslo, 2007.

11. Lamon, L.; von Waldow, H.; MacLeod, M.; Scheringer, M.; Marcomini, A.; Hungerbuhler, K. Modeling the global levels and distribution of polychlorinated biphenyls in air under a climate change scenario. *Environ. Sci. Technol.* **2009,** *43*, 5818-5824.

12. Ma, J.; Cao, Z. Quantifying the perturbations of persistent organic pollutants induced by climate change. *Environ. Sci. Technol.* **2010,** *44*, 8567-8573.

13. Ma, J.; Hung, H.; Tian, C.; Kallenborn, R. Revolatilization of persistent organic pollutants in the Arctic induced by climate change. *Nature Clim. Change* **2011,** *1*, 255-260.

14. Gouin, T.; Armitage, J. M.; Cousins, I. T.; Muir, D. C. G.; Ng, C. A.; Reid, L.; Tao, S. Influence of global climate change on chemical fate and bioaccumulation: The role of multimedia models. *Environ. Toxicol. Chem.* **2013,** *32*, 20-31.

15. Wöhrnschimmel, H.; MacLeod, M.; Hungerbühler, K. Emissions, fate and transport of persistent organic pollutants to the Arctic in a changing global climate. *Environ. Sci. Technol.* **2013,** *Just Accepted*.

16. Wu, S.; Mickley, L. J.; Jacob, D. J.; Rind, D.; Streets, D. G. Effects of 2000-2050 changes in climate and emissions on global tropospheric ozone and the policy-relevant background surface ozone in the United States. *J. Geophys. Res.* **2008,** *113*, D18312.

17. Pye, H. O. T.; Liao, H.; Wu, S.; Mickley, L. J.; Jacob, D. J.; Henze, D. K.; Seinfeld, J. H. Effect of changes in climate and emissions on future sulfate-nitrate-ammonium aerosol levels in the United States. *J. Geophys. Res.* **2009,** *114*, D01205.

18. Fiore, A. M.; Naik, V.; Spracklen, D. F.; Steiner, A.; Cionni, I.; Collins, W. J.; Dalsøren, S.; Eyring, V.; Folberth, G. A.; Ginoux, P.; Horowitx, L. W.; Josse, B.; Lamarque, J.-F.; MacKenzie, I. A.; Nagashima, T.; O'Connor, F. M.; Righi, M.; Rumbold, S. T.; Shindell, D. T.; Skeie, R. B.; Sudo, K.; Szopa, S.; Takemura, T.; Zeng, G. Global air quality and climate. *Chem. Soc. Rev.* **2012,** *41*, 6663-6683.

19. Bey, I.; Jacob, D. J.; Yantosca, R. M.; Logan, J. A.; Field, B.; Fiore, A. M.; Li, Q.; Liu, H. X.; Mickley, L. J.; Schultz, M. Global modeling of tropospheric chemistry with assimilated meteorology: Model description and evaluation. *J. Geophys. Res.* **2001,** *106*, 23,073-23,096.

20. Zelenyuk-Imre, A.; Imre, D.; Beranek, J.; Abramson, E. H.; Wilson, J.; Shrivastava, M. Synergy between secondary organic aerosols and long-range transport of polycyclic aromatic hydrocarbons. *Environ. Sci. Technol.* **2012,** *Just Accepted Manuscript*.

21. Heald, C. L.; Coe, H.; Jimenez, J. L.; Weber, R. J.; Bahreini, R.; Middlebrook, A. M.; Russell, L. M.; Jolleys, M.; Fu, T.-M.; Allan, J. D.; Bower, K. N.; Capes, G.; Crosier, J.; Morgan, W. T.; Robinson, N. H.; Williams, P. I.; Cubison, M. J.; DeCarlo, P. F.; Dunlea, E. J. Exploring the vertical profile of atmospheric organic aerosol: comparing 17 aircraft field campaigns with a global model. *Atmos. Chem. Phys.* **2011,** *11*, 12673-12696.

22. Friedman, C. L.; Pierce, J. R.; Selin, N. E. Assessing the influence of secondary organic aerosols on long-range atmospheric PAH transport. *Environ. Sci. Technol.* **2013,** *Submitted*.

23. Zhang, Y.; Tao, S. Global atmospheric emission inventory of polycyclic aromatic hydrocarbons (PAHs) for 2004. *Atmos. Environ.* **2009,** *43*, 812-819.

24. Park, R. J.; Jacob, D. J.; Chin, M.; Martin, R. V. Sources of carbonaceous aerosols over the United States and implications for natural visibility. *J. Geophys. Res.* **2003,** *108(D12)*, 4355.

25. Dachs, J.; Eisenreich, S. J. Adsorption onto aerosol soot carbon dominates gas-particle partitioning of polycyclic aromatic hydrocarbons. *Environ. Sci. Technol.* **2000,** *34*, 3690-3697.

26. Mackay, D.; Paterson, S. Evaluating the multimedia fate of organic chemics: A level III fugacity model. *Environ. Sci. Technol.* **1991,** *25*, 427-436.

27. Cousins, I. T.; Mackay, D. Strategies for including vegetation compartments in multimedia models. *Chemosphere* **2001,** *44*, 643-654.

28. Cousins, I. T.; Mackay, D. Transport parameters and mass balance equations for vegetation in Level III fugacity models. Internal report published on the website of the Canadian Environmental Modelling Centre (http://www.trent.ca/envmodel/). **2000**.

29. Lohmann, R.; Klanova, J.; Pribylova, P.; Liskova, H.; Yonis, S.; Bollinger, K. PAHs on a West-to-East transect across the Tropical Atlantic Ocean. *Environ. Sci. Technol.* **2013,** *Article ASAP*.

30. Nizzetto, L.; Lohmann, R.; Gioia, R.; Jahnke, A.; Temme, C.; Dachs, J.; Herckes, P.; Di Guardo, A.; Jones, K. C. PAHs in air and seawater along a North-South Atlantic transect: Trends, processes and possible sources. *Environ. Sci. Technol.* **2008,** *42*, 1580-1585.

31. Lohmann, R.; Gioia, R.; Jones, K. C.; Nizzetto, L.; Temme, C.; Xie, Z.; Schulz-Bull, D.; Hand, I.; Morgan, E.; Jantunen, L. Organochlorine pesticides and PAHs in the surface water and atmosphere of the North Atlantic and Arctic Ocean. *Environ. Sci. Technol.* **2009,** *45*, 5633-5639.

32. Baker, J. E.; Eisenreich, S. J. Concentrations and Fluxes of Polycyclic Aromatic-Hydrocarbons and Polychlorinated-Biphenyls across the Air-Water-Interface of Lake-Superior. *Environ. Sci. Technol.* **1990,** *24*, 342-352.

33. Nelson, E. D.; McConnell, L. L.; Baker, J. E. Diffusive exchange of gaseous polycyclic aromatic hydrocarbons and polychlorinated biphenyls across the air-water interlace of the Chesapeake Bay. *Environ. Sci. Technol.* **1998,** *32*, 912-919.

34. Bamford, H. A.; Offenberg, J. H.; Larsen, R. K.; Ko, F. C.; Baker, J. E. Diffusive exchange of polycyclic aromatic hydrocarbons across the air-water interface of the Patapsco River, an urbanized subestuary of the Chesapeake Bay. *Environ. Sci. Technol.* **1999,** *33*, 2138-2144.

35. Wu, S.; Mickley, L. J.; Leibensperger, E. M.; Jacob, D. J.; Rind, D.; Streets, D. G. Effects of 2000-2050 global change on ozone air quality in the United States. *J. Geophys. Res.* **2008,** *113*, D06302.

36. Sofowote, U. M.; Hung, H.; Rastogi, A. K.; Westgate, J. N.; Su, Y.; Sverko, E.; D'Sa, I.; Roach, P.; Fellin, P.; McCarry, B. E. The gas/particle partitioning of polycyclic aromatic hydrocarbons collected at a sub-Arctic site in Canada. *Atmos. Environ.* **2010,** *44*, 4919-4926.

37. IEA. International Energy Agency. World Energy Outlook 2011. **2011,** *Paris, France*.

38. Wenborn, M. J.; Coleman, P. J.; Passant, N. R.; Lymberidi, E.; Sully, J.; Weir, R. A. Speciated PAH inventory for the UK, AEA Technology Environment, Oxfordshire, UK. <http://www.airquality.co.uk/archive/reports/cat08/0512011419_REPFIN_all_nov.pdf>. **1999**.

39. GLC. Great Lakes Commission. Assessment of Benzo(a)pyrene Air Emissions in the Great Lakes Region: A report of the Great Lakes Regional Toxic Air Emissions Inventory Steering Committee. **2007**.

40. EPA, U. S. 1990 Emissions Inventory of Section 112(c)(6) Pollutants: Polycyclic Organic Matter (POM), TCDD, TCDF, PCBs, Hexachlorobenzene, Mercury, and Alkylated Lead: Final Resport, U.S. Environmental Protection Agency, Research Triangle Park, NC. Available from: <http://www.epa.gov/ttn/atw/112c6/final2.pdf>. **1998**.

41. IEA *International Energy Agency. World Energy Outlook 2010.*; Paris, France, 2010.

42. Bond, T. C.; Streets, D. G.; Yarber, K. F.; Nelson, S. M.; Woo, J. H.; Klimont, Z. A technology-based global inventory of black and organic carbon emissions from combustion. *J. Geophys. Res.-Atmos.* **2004,** *109*, (D14).

43. Zhang, Y. X.; Tao, S. Emission of polycyclic aromatic hydrocarbons (PAHs) from indoor straw burning and emission inventory updating in China. *Annals of New York Academy of Sciences* **2008,** *1140*, 218-227.

44. Shen, H.; Tao, S.; Wang, R.; Wang, B.; Shen, G.; Li, W.; Su, S.; Huang, Y.; Wang, X.; Liu, W.; Li, B.; Sun, K. Global time trends in PAH emissions from motor vehicles. *Atmos. Environ.* **2011,** *45*, 2067-2073.

45. Agrawal, H.; Welch, W.; Miller, J. W.; Cocker, D. R. Emissions measurements from a cruide oil tanker at sea. *Environ. Sci. Technol.* **2008,** *42*, 7098-7103.

46. Liu, Y.; Stanturf, J.; Goodrick, S. Trends in global wildfire potential in a changing climate. *Forest. Ecol. Manag.* **2010,** *259*, 685-697.

47. Scholze, M.; Knorr, W.; Arnell, N. W.; Prentice, I. C. A climate-change risk analysis for world ecosystems. *PNAS* **2006,** *103*, 13116-13120.

48. Krawchuk, M. A.; Moritz, M. A.; Parisien, M.-A.; Van Dorn, J.; Hayhoe, K. Global pyrogeography: The current and future distribution of wildfire. *PLoS ONE* **2009,** *4*, e5102.

49. Spracklen, D. V.; Mickley, L. J.; Logan, J. A.; Hudman, R. C.; Yevich, R.; Flannigan, M. D.; Westerling, A. L. Impacts of climate change from 2000 to 2050 on wildfire activity and carbonaceous aerosol concentrations in the western United States. *J. Geophys. Res.* **2009,** *114*, D20301.

50. Stocks, B. J.; Fosberg, M. A.; Lynham, T. J.; Mearns, L.; Wotton, B. M.; Yang, Q.; Jin, J.-Z.; Lawrence, K.; Hartley, G. R.; Mason, J. A.; McKenney, D. W. Climate change and forest fire potential in Russian and Canadian boreal forests. *Climatic Change* **1998,** *38*, 1-13.

51. Malevsky-Malevich, S. P.; Molkentin, E. K.; Nadyozhina, E. D.; Shklyarevich, O. B. An assessment of potential change in wildfire activity in the Russian boreal forest zone induced by climate warming during the twenty-first century. *Climatic Change* **2008,** *86*, 463-474.

52. Neilson, R. P.; Pitelka, L. F.; Solomon, A. M.; Nathan, R.; Midgley, G. F.; Fragoso, J. M. V.; Lischke, H.; Thompson, K. Forecasting regional to global plant migration in response to climate change. *BioScience* **2005,** *55*, 749-759.

53. Streets, D. G.; Bond, T. C.; Lee, T.; Jang, C. On the future of carbonaceous aerosol emissions. *J. Geophys. Res.* **2004,** *109*, D24212.

54. Williams, A.; O'Sullivan Darcy, A.; Wilkinson, A. *The future of Arctic enterprise: Long-term outlook and implications*; Smith School of Enterprise and the Environment, University of Oxford: Oxford, UK, 2011.

55. Hunsinger, E.; Howell, D. *Alaska Population Projections 2010-2035*; Alaska Department of Labor and Workforce Development: Juneau, Alaska, USA, 2012.

56. Thackray, C. P.; Friedman, C. L.; Selin, N. E. Parametric uncertainty analysis of PAH simulations using the GEOS-Chem atmospheric chemical transport model. *Environ. Sci. Technol.* **2013,** *To be submitted*.

57. Gusev, A.; MacLeod, M.; Bartlett, P. Intercontinental transport of persistent organic pollutants: a review of key findings and recommendations of the task force on hemispheric transport of air pollutants and directions for future research. *Atmos. Poll. Res.* **2012,** *3*, 463-465.

58. Daly, G. L.; Wania, F. Simulating the influence of snow on the fate of organic compounds. *Environ. Sci. Technol.* **2004,** *38*, 4176-4186.

59. AMAP *Arctic Pollution*; Oslo, 2009; p 83.

60. Galbán-Malagón, C.; Berojalbiz, H.; Ojeda, M.-J.; Dachs, J. The oceanic biological pump modulates the atmospheric transport of persistent organic pollutants to the Arctic. *Nat. Commun.* **2012,** *3:862*.

Climate change and emissions impacts on atmospheric PAH transport to the Arctic – Supporting Information

Carey L. Friedman[1], Yanxu Zhang[2] and Noelle E. Selin[3]

[1][Center for Global Change Science, Massachusetts Institute of Technology, Cambridge, Massachusetts]

[2][School of Engineering and Applied Sciences, Harvard University, Cambridge, Massachusetts]

[3][Engineering Systems Division and Department of Earth, Atmospheric, and Planetary Science, Massachusetts Institute of Technology, Cambridge, Massachusetts]

Correspondence to: C. L. Friedman (clf@mit.edu)

Table of Contents **Page**

Table of Contents, continued **Page**

Mean January 2000 PYR concentration (ng/m^3)	*Global*	*NH*	*ML*	*Arctic*
Using monthly average OH, O_3, OC, and BC	0.0694	0.123	0.145	0.0897
Using daily average OH, O_3, OC, and BC	0.0708	0.125	0.148	0.0899
% Difference	+1.9	+2.0	+2.1	+0.21

Table S1. Difference between global, northern hemisphere, northern hemisphere mid-latitude (5-60°N), and Arctic (60-90°N) mean PYR concentrations (ng m^{-3}) for January 2000 when monthly (top) versus daily (bottom) mean oxidant and aerosol concentrations are used as input to the PAH simulation. PYR was used as a test PAH, given its semivolatility and thus sensitivity to changes in both oxidants and particles.

Re-emissions model

Given minimal data on the global distribution of surface concentrations of PAHs and their exchange with the air, the re-emissions model is a simple steady-state level-III fugacity model. Surface concentrations are static, while partition coefficients are re-calculated dynamically on the atmospheric model time step, according to surface and air temperature changes. The re-emissions model has two components: a soil-air exchange model, and a vegetation-air exchange model.

Development of soil-air exchange model (derived primarily from Mackay and Paterson[1]; values of constants are given in Table S2):

Re-emissions from soils are generated as follows: (1) global soil concentration fields are created by multiplying annual simulated deposited mass for each PAH by its "soil deposition storage quotient" (i.e., number of years-worth of atmospheric deposition measured in top 5 cm of soils)[2], and distributing this mass throughout the top 5 cm; (2) air-soil fugacity gradients[1] are calculated using global soil organic carbon fractions generated with a version of the CASA biogeochemical model previously coupled to GEOS-Chem[3]; (3) fluxes and fugacity gradients are constrained to observations[4-6].

Soil storage quotients are 2.6 years for PHE, 10 years for PYR, and 9.4 years for BaP. Resulting soil concentrations were used for all four climate/emissions scenarios. A fraction of this concentration was assumed lost to degradation (at a rate of R_{deg}; Table S2). The fugacities (units of Pa) in the soil (F_{soil}) and the air (F_{air}) were then calculated[1]:

$$F_{soil} = \frac{C_{soil} \times R \times T_{surf}}{K_{SA}}$$

$$F_{air} = C_{air} \times R \times T_{air}$$

where R is the ideal gas constant (m^3 Pa K^{-1} mol^{-1}), T_{surf} is the Earth's surface skin temperature (K), and T_{air} is surface-level air temperature (K), and soil and air concentrations (C_{soil} and C_{air}, respectively) are in units of mol/m^3. K_{SA} (mol m^{-3} soil / mol m^{-3} air) is a soil-air partition coefficient calculated following previously described methods[7-9]:

$$K_{SA} = 1.5 \times f_{OC} \times K_{OA}$$

where f_{OC} is the fraction of organic carbon in the soil and K_{OA} is the temperature-dependent octanol-air partition coefficient. The f_{OC} is calculated by (1) combining annual mean carbon mass from all carbon pools simulated by the Global Terrestrial Mercury Model (GTMM), which is a version of the CASA biogeochemical model[10] coupled to the GEOS-Chem atmospheric mercury model[3]; (2) assuming this carbon mass extends to 30 cm[10] to create a soil carbon concentration; (3) assuming a mean soil bulk density[11] of 1300 kg/m^3 to calculate a soil organic carbon fraction (g C/g soil).

The soil-air flux ($Flux_{SA}$) is then calculated as follows:

$$Flux_{SA} = DS \times (F_{soil} - F_{air}) \times 24 \times MW_{PAH} \times 10^{12}$$

where $Flux_{SA}$ is in units of ng/m^2/day, DS is diffusivity through the soil (mol m^{-2} h^{-1} Pa^{-1}), and MW_{PAH} is the PAH molecular weight (kg/mol).

DS is calculated by:

$$DS = \frac{1}{\left(1/DSA + PL/(DAD + DWD)\right)}$$

where DSA is the air-side boundary layer diffusion parameter (mol/h/Pa;), PL is the soil diffusion path length (m), DAD is the diffusion parameter between soil particles and soil air (mol/h/Pa), and DWD is the diffusion parameter between soil pore water and particles (mol/h/Pa). Diffusion parameters are calculated as follows:

$$DSA = K_{SA} Z_{air}$$

$$DAD = BA \times Z_{air}$$

$$DWD = BW \times Z_{water}$$

where BA is the molecular diffusivity in air (m^2/h), BW is the molecular diffusivity in water (m^2/h), and Z_{air}, Z_{soil}, and Z_{water} are the fugacity capacities (mol/m^3/Pa) in air, soil, and water:

$$Z_{air} = \frac{1}{RT_{air}}$$

$$Z_{water} = \frac{1}{K_{AW} R T_{surf}}$$

Net fluxes (the sum of monthly mean positive and negative fluxes), when positive, are added to primary emissions to calculate total emissions.

Development of vegetation-air exchange model (derived primarily from Cousins and Mackay[1, 12, 13]; values of constants are given in Table S2):

Re-emissions from vegetation are generated by considering fugacity gradients between leaf surfaces and air. Vegetation PAH concentrations (C_{leaf}) were generated by distributing the annual simulated deposited mass for each PAH throughout a general leaf surface thickness (d_{leaf}) of 2e-6 m and an arbitrary leaf surface area such that concentrations were of the same order of magnitude as those previously reported[14, 15] (i.e., PHE concentrations in the hundreds, PYR in the tens, and BaP between 1 and 10). The resulting concentrations were used for all four climate/emissions scenarios. A temperature-dependent octanol-water partition coefficient (K_{OW}, unitless) was then estimated from K_{OA} and K_{AW}:

$$K_{OW} = K_{OA} K_{AW}$$

and a leaf surface – air partition coefficient (K_{LA}) was also calculated from the K_{OA} by assuming an octanol-equivalent volume fraction[12] (f_{oct}) in the leaf surface of 0.8:

$$K_{LA} = f_{oct} K_{OA}$$

Fugacities (Pa) in the leaf surface (F_{leaf}) and air (as above) were then calculated from their respective concentrations (mol/m^3):

$$F_{leaf} = \frac{C_{leaf} \times R \times T_{surf}}{K_{LA}}$$

The vegetation-air flux (ng/m^2/d) was derived from the fugacity gradient:

$$Flux_{VA} = DLA \times (F_{leaf} - F_{air}) \times 24 \times MW_{PAH} \times 10^{12}$$

where DLA (mol/Pa/h) is the diffusion parameter for gas phase leaf surface – air transfer. DLA is calculated by:

$$DLA = \frac{1}{1/DC + 1/DAB_f}$$

where DC (mol/Pa/h) is cuticle diffusions and DAB_f (mol/Pa/h) is the boundary layer diffusion. DC is given by:

$$DC = As \times L \times Uc \times Z_{leaf}$$

where As is the area of the land surface (m^2), L is the leaf area index (m^2/m^2), Uc is the cuticle mass transfer coefficient (m/h), and Z_{leaf} is the fugacity capacity of the leaf ($mol/m^3/Pa$). Uc is determined by:

$$Uc = 3600 \times Pc \times 1/K_{AW}$$

where Pc is the cuticle permeance (m/s) given by:

$$\log(Pc) = \frac{((0.704 \times \log(K_{OW}) - 11.2) + (-3.47 - 2.79 \times \log(MW_{PAH}) + 0.970 \times \log(K_{OW}))}{2}$$

Z_{leaf} is calculated as follows:

$$Z_{leaf} = \frac{K_{LA}}{RT_{surf}}$$

DAB_f is given by:

$$DAB_f = UAB_f \times Z_{air}$$

where UAB_f is a mass transfer coefficient for surface-air boundary layer diffusion (m/h) and Z_{air} is as above ($mol/m^3/Pa$).

Vegetation emissions (kg/s) are then calculated by:

$$Em_{veg} = \frac{Flux_{VA} \times A \times LAI}{24 \times 3600 \times 10^{12}}$$

where A is the area of the grid box (m^2) and LAI is the leaf area index (cm^2 leaf surface/cm^2 GEOS-Chem gridbox) given by the NOAA Advanced Very High Resolution Radiometer (AVHRR) satellite. Emissions are added to primary emissions when $Flux_{VA}$ is positive.

Vegetation flux observations are, to our knowledge, unavailable in the literature.

Compound	Metric	Lat.	Long.	Observation period	Observation Values	Simulated Value	Observation reference
PHE	Fugacity ratio (unitless)	41.4-42.4 N	2.7 W-2.1 E	6/2006	10 to 600*	37	(a)
				11/2006		3	(a)
				9/2007		19	(a)
	Flux (ng/m^2/day)	38.5 – 41.1 N	115.4 – 118.1 E	Fall 2007	-13 (median); -99 to 268 (range)	-3	(b)
				Winter 2007	-115 (median); -348 to -10 (range)	-62	(b)
				Spring 2008	-11 (median); -86 to 250 (range)	27	(b)
				Summer 2008	92 (median); 6 to 796 (range)	218	(b)
	Fugacity fraction (unitless)	22 – 23.8 N	112.4 – 114.2 E	9/2001	0.02 – 0.11	0.98	(c)
PYR	Fugacity ratio (unitless)	41.4-42.4 N	2.7 W-2.1 E	6/2006	10-150*	46	(a)
				11/2006		2	(a)
				9/2007		23	(a)
	Flux (ng/m^2/day)	38.5 – 41.1 N	115.4 – 118.1 E	Fall 2007	-3 (median); -10 to 6 (range)	-2	(b)
				Winter 2007	-11 (median); -37 to -0.8 (range)	-5	(b)
				Spring 2008	-7 (median); -25 to 5 (range)	1	(b)
				Summer 2008	2 (median); -12 to 31 (range)	45	(b)
	Fugacity fraction	22 – 23.8 N	112.4 – 114.2 E	9/2001	0-0.08	0.97	(c)
BaP	Fugacity ratio (unitless)	41.4-42.4 N	2.7 W-2.1 E	6/2006	0.9-3*	0.11	(a)
				11/2006		0.07	(a)
				9/2007		0.03	(a)
	Flux (ng/m^2/day)	38.5 – 41.1 N	115.4 – 118.1 E	Fall 2007	-0.01 (median); -0.04 to NA (range)	-0.03	(b)
				Winter 2007	-0.02 (median); -0.07 to NA (range)	-0.001	(b)
				Spring 2008	-0.01 (median); -0.06 to NA (range)	-0.02	(b)
				Summer 2008	-0.01 (median); -0.04 to NA (range)	-0.07	(b)

Table S2. Comparison of simulated re-emissions fluxes, fugacity ratios, and fugacity fractions to observed. Positive fluxes are in the direction of soil-to-air, negative fluxes are air-to-soil. Fugacity ratios are defined as the fugacity in the soil divided by the fugacity in the air. Fugacity fractions are defined as the fugacity in the soil divided by the sum of the fugacities in soil and air. Observations are from (a) Cabrerizo et al., 2011[5]; (b) Wang et al., 2011[4]; and (c) Liu et al., 2011[6]. The evaluation of the flux model was completed

using NASA GEOS5 meteorology and for all observation data except those from Liu et al., simulated values were derived from the meteorological months corresponding to the reported sampling periods. For comparisons to Liu et al. data, mean simulated values from September 2005-2009 were used. *Values are approximations derived from plots in cited work. Our simulations capture the reported seasonal variation (largest fugacity ratios in June, followed by September, and then November). N.A. = not available.

Parameter	Description	PHE	PYR	BaP	Ref
log K_{OA}	Octanol-air partition coefficient	7.64	8.86	11.48	a
log K_{BC}	Black carbon-air partition coefficient	10.0	11.0	13.9	b
log K_{AW}	Air-water partition coefficient	-2.76	-3.27	-4.51	a
$\Delta_{OA}H$ (kJ/mol)	Enthalpy of phase transfer from gas phase to OC	-74	-87	-110	c
$\Delta_{BC}H$ (kJ/mol)	Enthalpy of phase transfer from gas phase to BC	-74	-87	-110	c
$\Delta_{AW}H$ (kJ/mol)	Enthalpy of phase transfer from water to air	47	43	43	c
k_{OH} (cm^3/molec/s)	Reaction rate constant for oxidation of gas phase with OH	2.70e-11	5.00e-11	5.00e-11	d, e
A (s^{-1})	Kinetic parameter for ozonation of PAHs on octanol and decanol	5e-4	7e-4	5.5e-3	f
B (molec/cm^3)	Kinetic parameter for ozonation of PAHs on octanol and decanol	2.15e15	3e15	2.8d15	f
k_{SA} (m/h)	Air-side mass transfer coefficient over soil	1.0	1.0	1.0	g
BA (m^2/h)	Molecular diffusivity in air	0.04	0.04	0.04	g
BW (m^2/h)	Molecular diffusivity in water	4e-6	4e-6	4e-6	g
R_{deg} (h^{-1})	Degradation rate in soil	3.5e-5	3.5e-5	3.5e-5	g
PL (m)	Soil path length (half of soil depth)	0.025	0.025	0.025	g
UAB_f (m/h)	Leaf surface transfer velocity	9	9	9	h
ρ_{oct} (kg/m^3)	Density of octanol	820			b
ρ_{BC} (kg/m^3)	Density of BC	1000			b
τ_{OCBC} (d)	Lifetime of hydrophobic OC and BC before converting to hydrophilic	1.15			i
f_{oct}	Volume fraction of octanol equivalent in leaf surface	0.8			g
d_{leaf} (m)	Leaf surface thickness	2e-6			h

Table S3. Physicochemical constants used in model for PHE, PYR, and BaP. References: (a) Ma et al., 2010[16]; (b) Lohmann and Lammel, 2004[17]; (c) Schwarzenbach et al., 2003[18]; (d) Brubaker and Hites, 1998[19]; (e) U.S. EPA Episuite software[20]; (f) Kahan et al., 2006[21] (g) Mackay and Paterson, 1991[1]; (h) Cousins and Mackay, 2001[12]; (i) Park et al., 2003[22].

Particles and oxidants under FE OC and BC emissions result from four source types: biofuel, biomass burning (including wildfires), fossil fuel, and biogenic (OC only)[22]. For FE and FCFE simulations, we use 2050 anthropogenic OC and BC emissions (i.e., from biofuel, biomass burning, and fossil fuel sources) estimated under the IPCC's A1B scenario based on previously reported methods[23-26]. The control emissions, minimum and maximum scaling factors for future global emissions, and the mean percent changes in global OC and BC emissions are shown in Table S3. Declining emissions generally result in decreases in OC and BC concentrations.

Surface O_3 and OH concentrations increase, mostly from changes in anthropogenic NO_X and methane. Model simulations for the purpose of investigating O_3 and OH concentrations under future emissions and climate scenarios have been described extensively previously[24, 27]. Here we reproduce a summary of global O_3 precursor emissions under the control simulation, their scaling factors for 2050, and the mean percent change in total emissions in 2050 (Table S4)[24]. In addition to the species in Table S4, global mean methane concentrations are specified at 1750 ppb with a 5% interhemispheric gradient, based on observations. As methane is projected to rise to 2400 ppb by 2050 in the A1B scenario, a globally uniform methane concentration of 2400 ppb is used in the model for all future anthropogenic emissions scenarios.

Global surface concentrations in the control and future emissions scenarios are summarized in Figs. S5-S8 and Table S5.

Emissions source	*Control (Mg)*	*Scaling factors (Min-Max)*	*% Δ Global, 2050-2000*
		BC	
Biofuel	1.6×10^6	0.179 - 1.726	-60
Biomass burning	1.7×10^6	0.360 - 1.851	-14
Fossil fuel	3.0×10^6	0.212 - 2.977	-32
		OC	
Biofuel	6.3×10^6	0.160 - 1.615	-58
Biomass burning	1.6×10^7	0.354 - 1.702	-18
Fossil fuel	3.0×10^6	0.217 - 1.174	-64

Table S4. Global annual emissions of particles under the control (2000) simulation, range of growth factors for 2050 FE and FCFE scenarios (depending on region), and resulting change in global emissions for 2050.

Emissions source	*Control (Mg)*	*Scaling factors (Min-Max)*	*% Δ Global, 2050-2000*
		NO_x (emissions of N)	
Biofuel	2.2×10^6	0.150 - 1.844	-5
Biomass burning	6.5×10^6	0.038 - 6.000	+25
Fertilizer	0.5×10^6	0.748 - 24.833	+80
Fossil fuel	24.6×10^6	0.597 - 18.354	+90
		CO	
Biofuel	176×10^6	0.160 - 1.846	-4%
Biomass burning	459×10^6	0.025 - 13.381	+63%
Fossil fuel	381×10^6	0.416 - 11.862	-5%
		Non-methane volatile organic compounds (NVMOCs; emissions of C)	
Anthropogenic	43×10^6	0.454 - 9.033	+130
Biomass burning	10×10^6	0.025 - 15.250	+66

Table S5. Global annual emissions of O_3 precursors under the control (2000) simulation, range of growth factors for 2050 FE and FCFE scenarios (depending on region), and resulting change in global emissions for 2050.

Particles and oxidants under FC Concentrations of OC, BC, O_3, and OH vary with FC due to changes in biogenic emissions (OC), chemical precursors (O_3 and OH), and meteorology (all). OC emissions increase by 2%. Briefly, the FC simulation considers changes to natural emissions of O_3 precursors, including nonmethane volatile organic compounds (NMVOCs) from vegetation, and NO_x from lightning and soil. These emissions are calculated within the model based on meteorology and hence change with climate scenario. Biogenic emissions of NMVOCs are influenced by temperature and solar radiation. Isoprene emissions increase by 25%, while all other NMVOC emissions increase by 20%. Lightning NO_x, a function of deep convective cloud top, increases by 18% globally, while soil NO_x emissions, a function of vegetation type, temperature, precipitation, fertilizer use, and leaf area index, increase by 8%. The model does not account for stratosphere-troposphere exchange of O_3. The effect of climate on global OH and O_3 has been discussed in detail by Wu et al.[24]

Together, emissions and meteorological changes result in lower surface-level OC and BC and small decreases in OH and O_3 under FC. These changes are summarized in Figs. S5-S8, Table S5).

Simulation			
Control Concentration	*FE (%Δ)*	*FC (%Δ)*	*FCFE (%Δ)*
OC (μg/m^3)			
0.056	-22	-18	-42
BC (μg/m^3)			
0.022	-30	-7	-38
OH (molec/cm^3)			
1e6	+4	-1	+5
O_3 (ppbv)			
34	+16	-2	+14

Table S6. Global surface concentrations of particles (OC and BC) and oxidants (OH and O_3) in the control, and percent change under each future scenario.

	% of total present-day emissions												Future anthropogenic emissions scaling factors (% Δ)				Total 2050 emissions and %Δ from control					
	PHE				PYR				BaP				Same for all PAHs				PHE		PYR		BaP	
Source region	Biomass burning	Vehicle use	Domestic coal	Coke production	Biomass burning	Vehicle use	Domestic coal	Coke production	Biomass burning	Vehicle use	Domestic coal	Coke production	Biomass burning	Vehicle use	Domestic coal	Coke production	Pres. (Mg)	% Δ	Pres. (Mg)	% Δ	Pres. (Mg)	% Δ
E. Asia	60	1	12	19	68	1	7	18	59	1	12	24	-60	-76	-60	-28	16,224	-10	6,501	-9	1,501	-11
S. Asia	85	1	1	<1	83	1	1	<1	89	1	2	1	-6	+13	-6	-28	18,096	-52	6,811	-51	1,204	-55
Europe	39	7	9	3	43	8	6	4	40	4	12	7	0	-98	0	+46	3,814	-6	1,191	-6	268	-1
N. America	22	12	2	1	27	13	1	1	27	10	3	3	0	-99	0	+75	3,020	-11	925	-12	161	-8
Russia	6	4	13	4	5	4	9	5	5	3	18	10	0	-98	0	+75	1,155	-1	382	-1	80	+5

Table S7. Contribution of different anthropogenic source activities to present-day total PAH emissions, factors for scaling anthropogenic emissions to 2050 for each source activity, and present-day total emissions and 2050 changes. Blue cells mark a decrease in emissions; red marks an increase.

	% of total present-day emissions due to wildfire			Future scaling factor (%)	Change in total emissions (% Δ)		
Source region	PHE	PYR	BaP	(all PAHs)	PHE	PYR	BaP
East Asia	1	1	<1	+25	0	0	0
South Asia	9	11	6	+50	+5	+6	+3
Europe	1	1	<1	+200	+2	+1	+1
North America	13	18	10	+88	+12	+16	+9
Russia	24	30	14	+15	+4	+4	+2

Table S8. Contribution of wildfire to present-day emissions, future climate wildfire emissions scaling factors, and 2050 changes due to wildfire.

Sensitivities to assumptions regarding wildfire emissions changes under FC

Given lack of projections for future wildfire activity in East Asia and Russia, we assume wildfire emissions in East Asia increase by half the increase in South Asia, and emissions in Russia increase by half the greatest predicted increase in annual dangerous fire days. These assumptions result in no change in East Asian wildfire emissions from 2000 to 2050, and a small increase in wildfire emissions in Russia from 2000 to 2050 (+2% to +4%; Table S7). If we adjust the scaling factors of these regions by +/-50%, given recent studies finding uncertainties in wildfire emissions within this range[28], we still find no impact on East Asian emissions, reflecting the low contribution of wildfire to total emissions in this region. Adjusting the scaling factor in Russia, however, can increase or decrease the 2000-2050 changes shown in Table S7 by up to 17% (for PYR). In other words, with a +/-50% certainty in the wildfire emissions scaling factors, 2000-2050 Russian emissions could either decrease by as much as 13%, or increase by as much as 21%. Russian emissions, however, account for only a small portion of the global inventory. For example, if we consider only the regions that we scale, Russian emissions account for just 2-3% of the total. Thus, +/-50% changes in Russian emissions projections have virtually no impact on the total 2000-2050 change in emissions under FC (<1%).

	Simulation			
Emissions	***Control (Mg)***	***FE (%Δ)***	***FC (%Δ)***	***FCFE (%Δ)***
		PHE		
Primary (kg)	61,000	-17	+2	-15
Re-emissions: Soil (kg)	12,000	+1	+23	+24
Re-emissions: Vegetation (kg)	180	+80	+28	+139
Total (kg)	72,000	-14	+5	-8
Re-emissions/Total	16%	+3	+3	+6
		PYR		
Primary (kg)	21,000	-18	+2	-16
Re-emissions: Soil (kg)	1800	+1	+28	+29
Re-emissions: Vegetation (kg)	2.3	+154	+33	+274
Total (kg)	23,000	-17	+4	-12
Re-emissions/Total	8%	+2	+2	+4
		BaP		
Primary (kg)	4200	-20	+1	-19
Re-emissions: Soil (kg)	0.32	+13	+48	+67
Re-emissions: Vegetation (kg)	7.4e-10	-63	+214	-52
Total (kg)	4200	-20	+1	-19
Re-emissions/Total	1%	+<1	+<1	+1

Table S9. Global primary, re-, and total annual emissions (kg) in the control and percent change in future simulations. Also shown is percent re-emissions of total, and change in percentage for future simulations.

	PHE			PYR			BaP			
Parameter	Used in model	Lower bound	Upper bound	Used in model	Lower bound	Upper bound	Used in model	Lower bound	Upper bound	Associated References
log K_{OA}	7.64	7.6	7.68	8.86	8.7	8.86	11.48	11.1	11.56	1, 2, 3
log K_{BC}*	10.0	9.24	10.1	11.0	10.45	11.04	13.9	12.9	14.1	4
log K_{AW}	-2.76	-3.0	-2.64	-3.27	-3.34	-3.15	-4.51	-4.85	-4.51	1, 5
Δ_{OA}H (kJ/mol)	-74	-80.62	-52.97	-87	-87.79	-75.89	-110	-110	-85	5, 6
Δ_{BC}H (kJ/mol)	-74	-80.62	-52.97	-87	-87.79	-75.89	-110	-110	-85	5, 6
Δ_{AW}H (kJ/mol)	47	30	60	43	30.5	56	43	43	43	5, 6
k_{OH} (cm^3/molec/s)	2.70e-11	1.3e-11	3.1e-11	5.00e-11	2.03e-11	2.92e-10	5.00e-11	5.00e-11	2.65e-10	7, 8, 9, 10

Table S10. Physicochemical parameters dominating PAH behavior within the atmospheric model: those used within the model and their lower and upper literature-derived values. *Upper and lower limits are calculated using a ratio of reported minimum and maximum $K_{BC\text{-}water}$ partition coefficients and minimum and maximum K_{AW}s. Associated references for this row include sources for both these partition coefficients.

References: (1) Ma et al., 2010[16]; (2) Beyer et al., 2002[29]; (3) Odabasi et al., 2006[30]; (4) Lohmann and Lammel, 2004[17]; (5) Shiu and Ma, 2000[31]; (6) Schwarzenbach et al., 2003[18]; (7) Brubaker and Hites, 1998[19]; (8) U.S. EPA Episuite software[20]; (9) NIST (http://webbook.nist.gov/cgi/cbook.cgi?ID=C50328&Mask=20#Ion-Energetics); (10) Bierman[32]

	Simulation			
	Control (ng m^{-3})	**FE (%Δ)**	**FC (%Δ)**	**FCFE (%Δ)**
PHE				
Global	0.18	-21	+5	-17
NH	0.30	-23	+4	-19
ML	0.36	-24	+4	-19
Arctic	0.15	-6	-2	-8
PYR				
Global	0.041	-25	+2	-23
NH	0.069	-28	+1	-26
ML	0.082	-29	+1	-26
Arctic	0.025	-6	-2	-7
BaP				
Global	0.022	-35	-3	-37
NH	0.039	-37	-3	-38
ML	0.048	-37	-3	-38
Arctic	6.7e-3	-7	-1	-8

Table S11. Global, northern hemisphere, northern hemisphere mid-latitude (5-60°N), and Arctic (60-90°N) mean concentrations (ng m^{-3}) in the present-day control and percent change for each future simulation.

	Simulation			
	Control Deposition/Emissions (kg/kg)	***FE (%Δ)***	***FC (%Δ)***	***FCFE (%Δ)***
PHE				
Gas dry	9%	-11	+2	-10
Particle dry	<1%	-28	-15	-37
Gas wet	<1%	-12	-2	-16
Particle wet	<1%	-56	-10	-62
TOTAL	9%	-11	+1	-11
PYR				
Gas dry	20%	-7	+4	-3
Particle dry	1%	-38	-15	-45
Gas wet	<1%	-9	-1	-11
Particle wet	<1%	-58	-10	-63
TOTAL	22%	-9	+3	-6
BaP				
Gas dry	7%	+25	+20	+47
Particle dry	12%	-20	-4	-24
Gas wet	1%	+15	+12	+25
Particle wet	10%	-28	-2	-31
TOTAL	30%	-10	+3	-7

Table S12. Global deposition (kg) normalized to total (primary + re-) emissions (kg) for each PAH in the control simulation, and the percent change in this ratio for future scenarios.

	Simulation			
	Control Oxidation/Emissions (kg/kg)	***FE (%Δ)***	***FC (%Δ)***	***FCFE (%Δ)***
PHE				
OH oxidation (gas)	90%	+2	-<1%	+2
O_3 oxidation (particles)	<1%	-<1%	-<1%	-<1%
TOTAL	90%	+2	-<1%	+2
PYR				
OH oxidation (gas)	78%	+2	-1	+1
O_3 oxidation (particles)	<1%	-<1%	-<1%	-<1%
TOTAL	78%	+2	-<1%	+2
BaP				
OH oxidation (gas)	41%	+7	+2	+9
O_3 oxidation (particles)	28%	-4	-3	-7
TOTAL	69%	+4	-1	+3

Table S13. Global oxidation (kg) normalized to total (primary + re-) emissions (kg) for each PAH in the control simulation, and the percent change in this ratio for future scenarios.

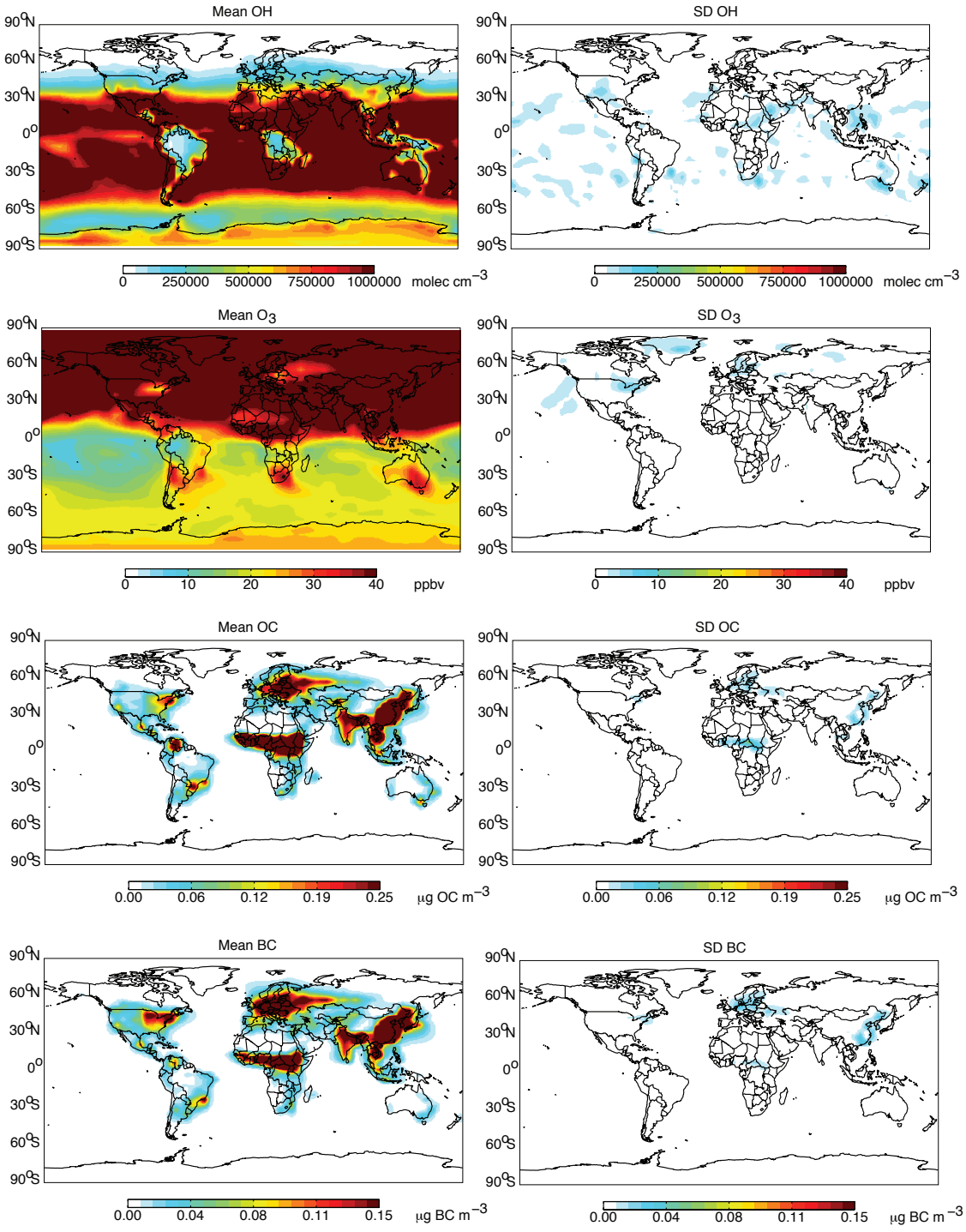

Figure S1. Monthly (January 2000) mean oxidant and aerosol concentrations when averaged over daily values (left panel) and associated standard deviations (right panel). Standard deviations suggest only minor variation in concentrations within a given month for each species. See Table S1 for the effects of averaging on mean PAH concentrations.

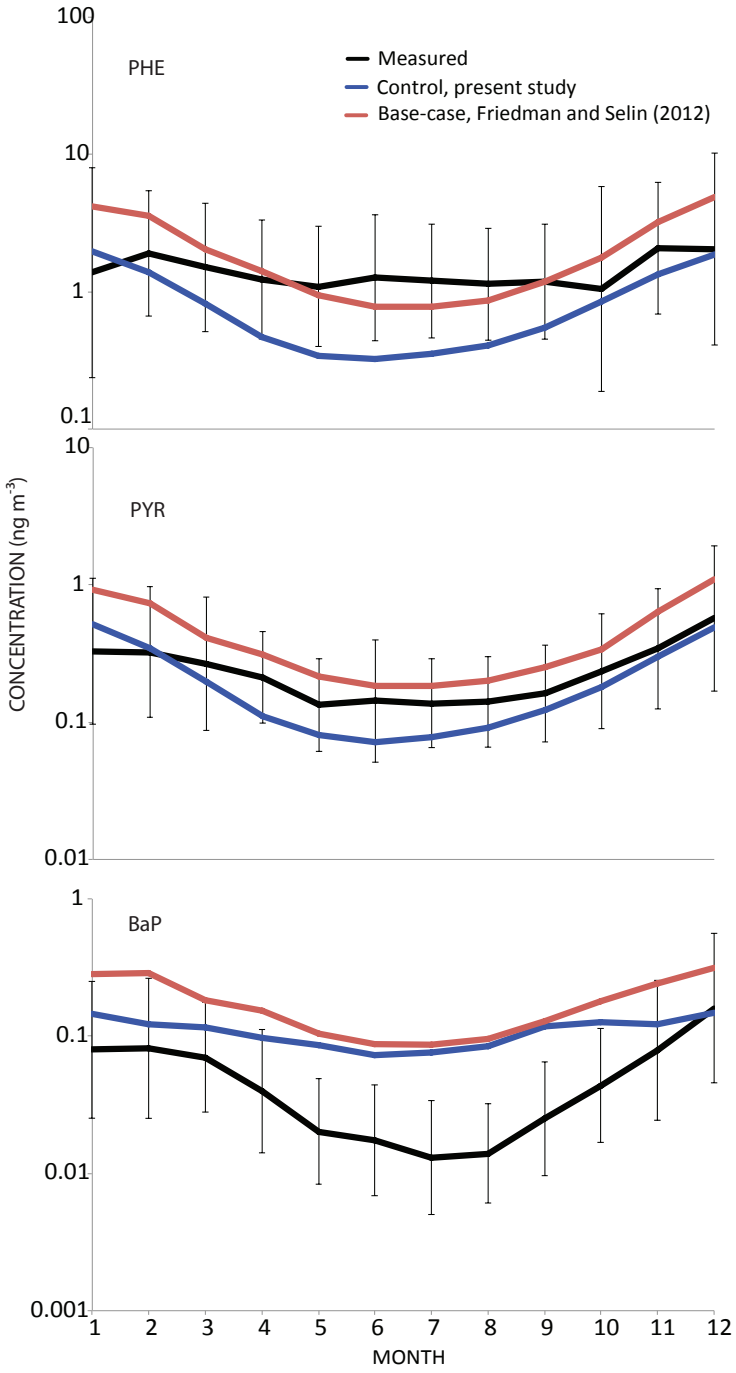

Figure S2. Comparison of non-urban mid-latitude concentrations from the control simulation in the present study to observations and simulated concentrations from Friedman and Selin[33]. Concentrations are monthly geometric means (+/- 1SD) from the non-urban mid-latitude sites (n=15 for PHE, PYR; n=16 for BaP) presented in Table 1 of Friedman and Selin.

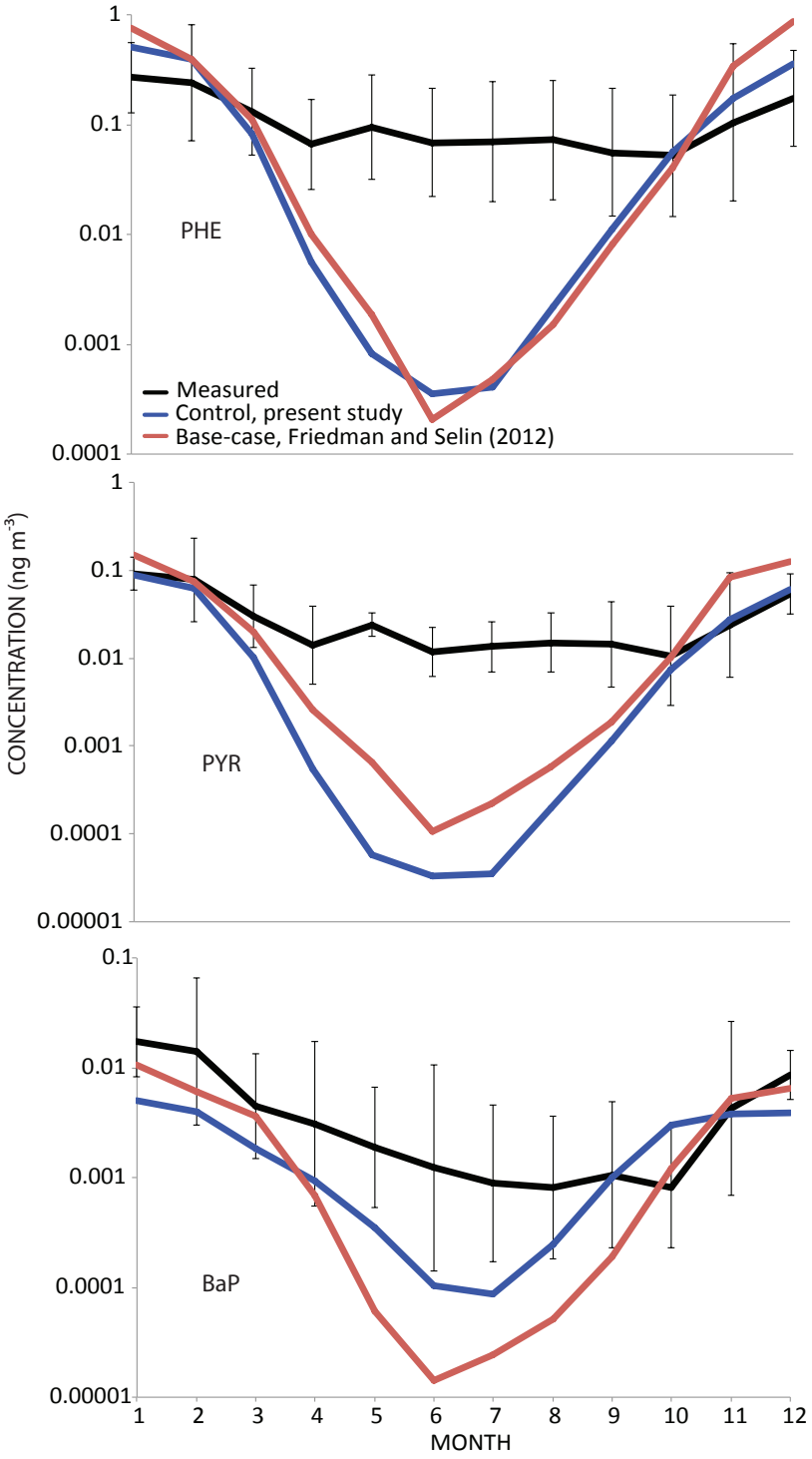

Figure S3. Comparison of Arctic concentrations from the control simulation in the present study to observations and simulated concentrations from Friedman and Selin[33]. Concentrations are monthly geometric means (+/- 1SD) from Arctic sites (n=3) presented in Table 1 of Friedman and Selin[33].

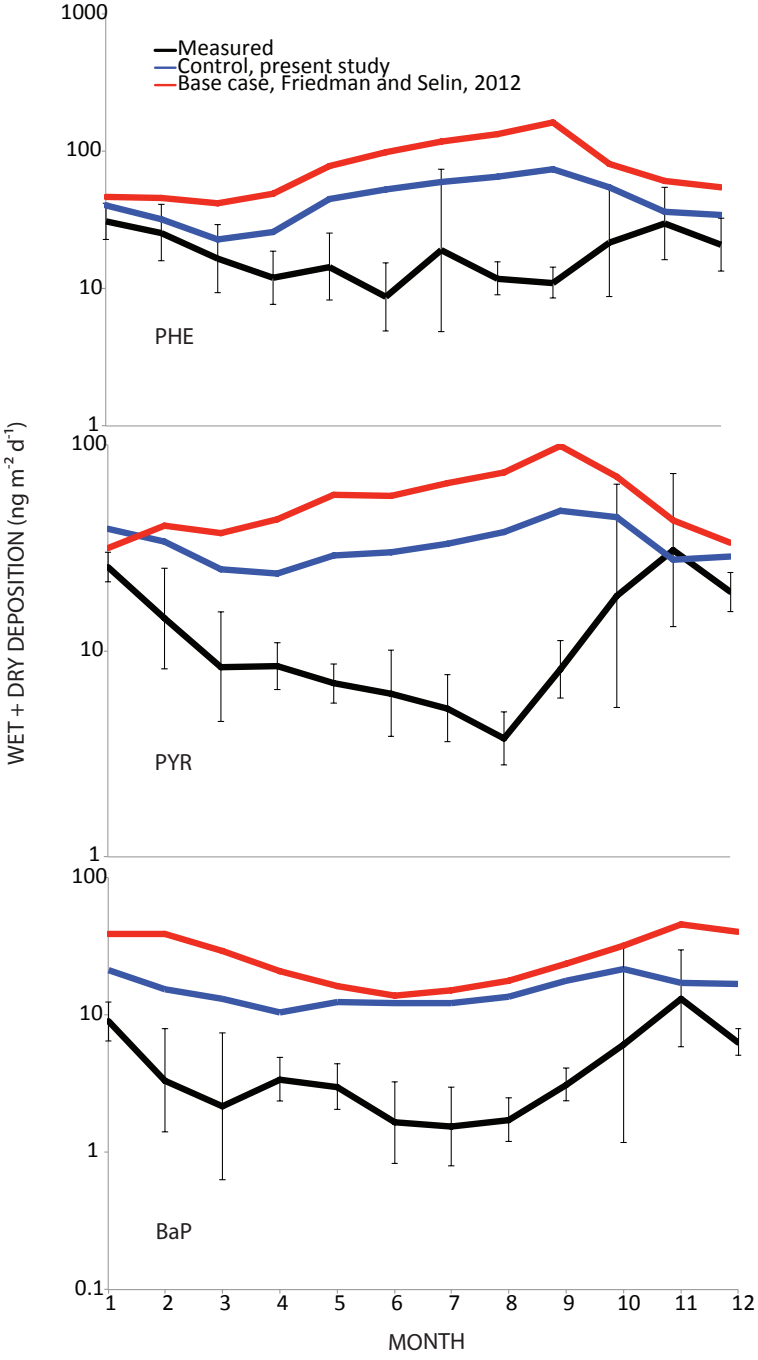

Figure S4. Comparison of deposition from the control simulation in the present study to observations and simulated deposition from Friedman and Selin[33]. Deposition values are monthly geometric means (+/- 1SD) from EMEP sites routinely reporting deposition (n=3) presented in Table 1 of Friedman and Selin[33].

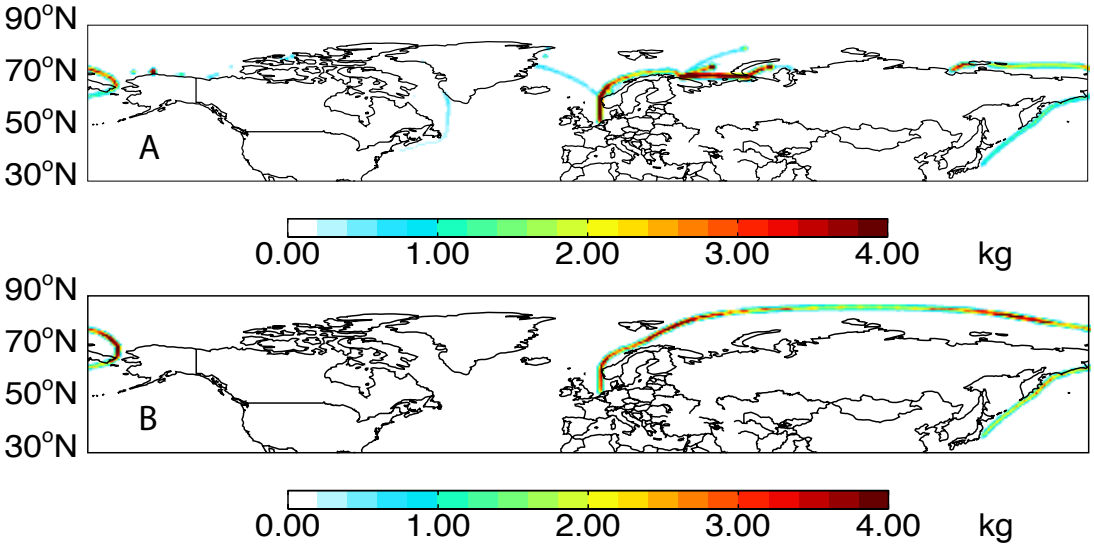

Figure S5. (A) Annual average of monthly emissions from 2050 projected shipping related to oil and gas; (B) average of monthly emissions from July - November 2050 projected transit shipping. Transit shipping is not projected to take place in the Arctic outside of these months.[34]

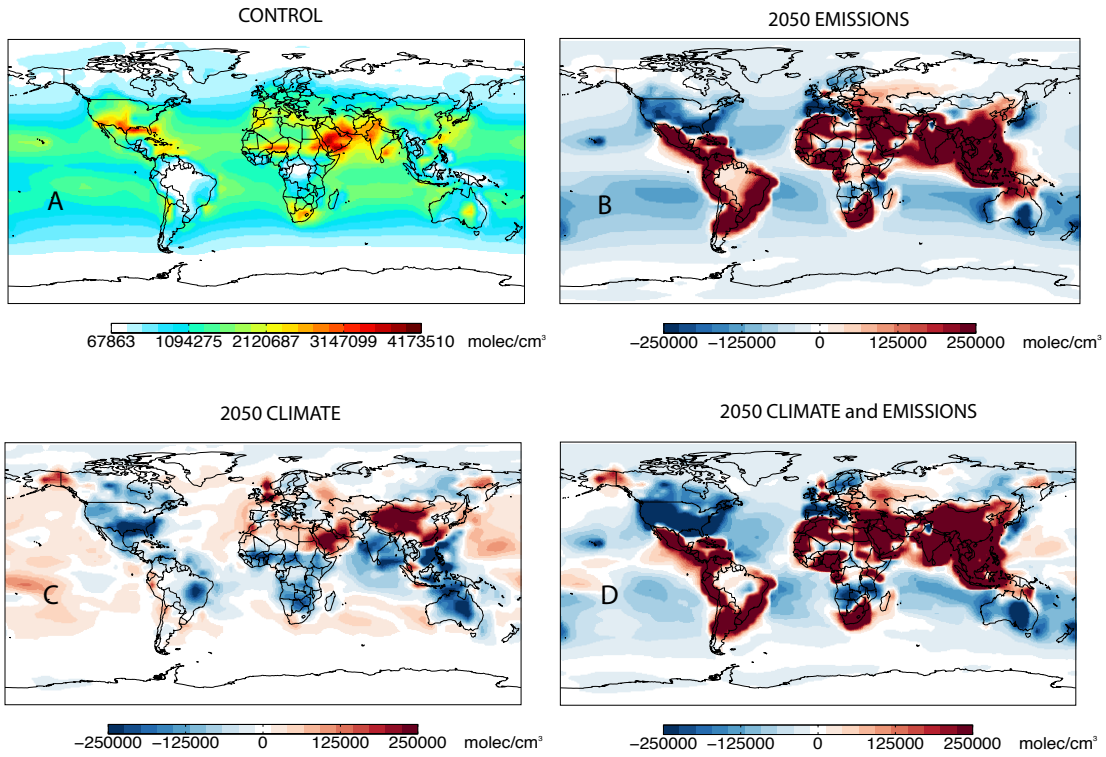

Figure S6. Global concentrations of OH under (A) the control simulation and difference in concentration between the control and simulations under (B) future emissions; (C) future climate, and; (D) future climate and future emissions. Red marks an increase in concentrations, blue marks a decrease.

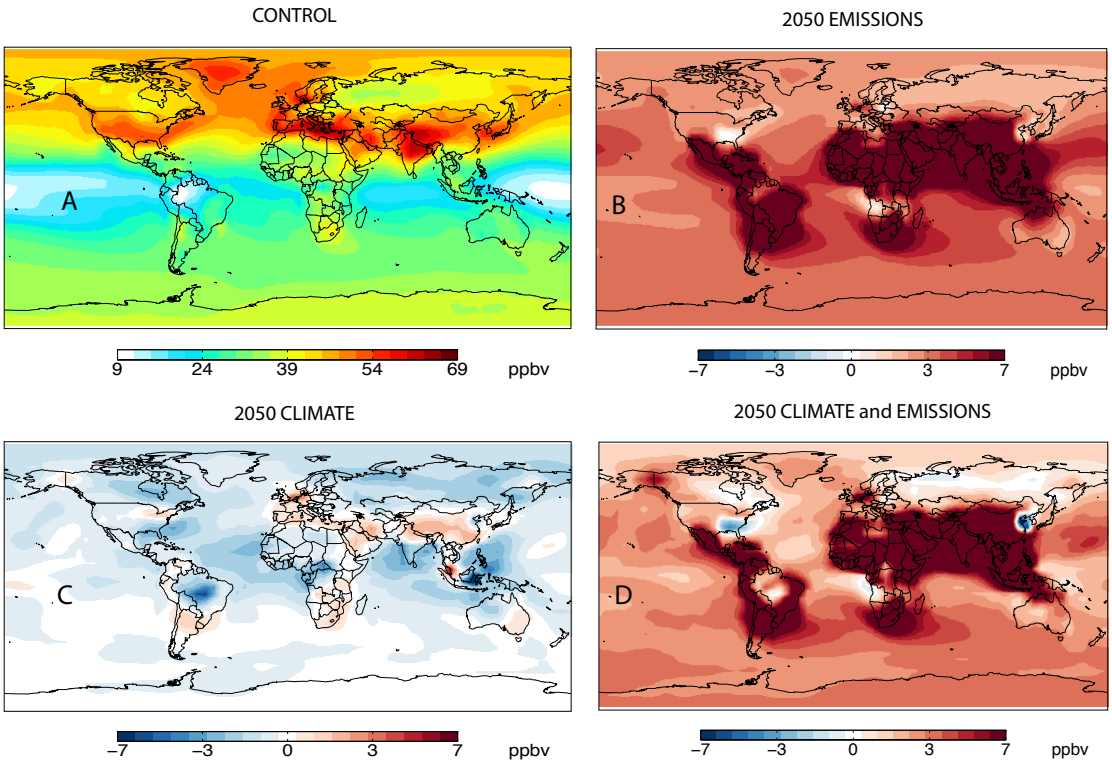

Figure S7. Global concentrations of O_3 under (A) the control simulation and difference in concentration between the control and simulations under (B) future emissions; (C) future climate, and; (D) future climate and future emissions. Red marks an increase in concentrations, blue marks a decrease.

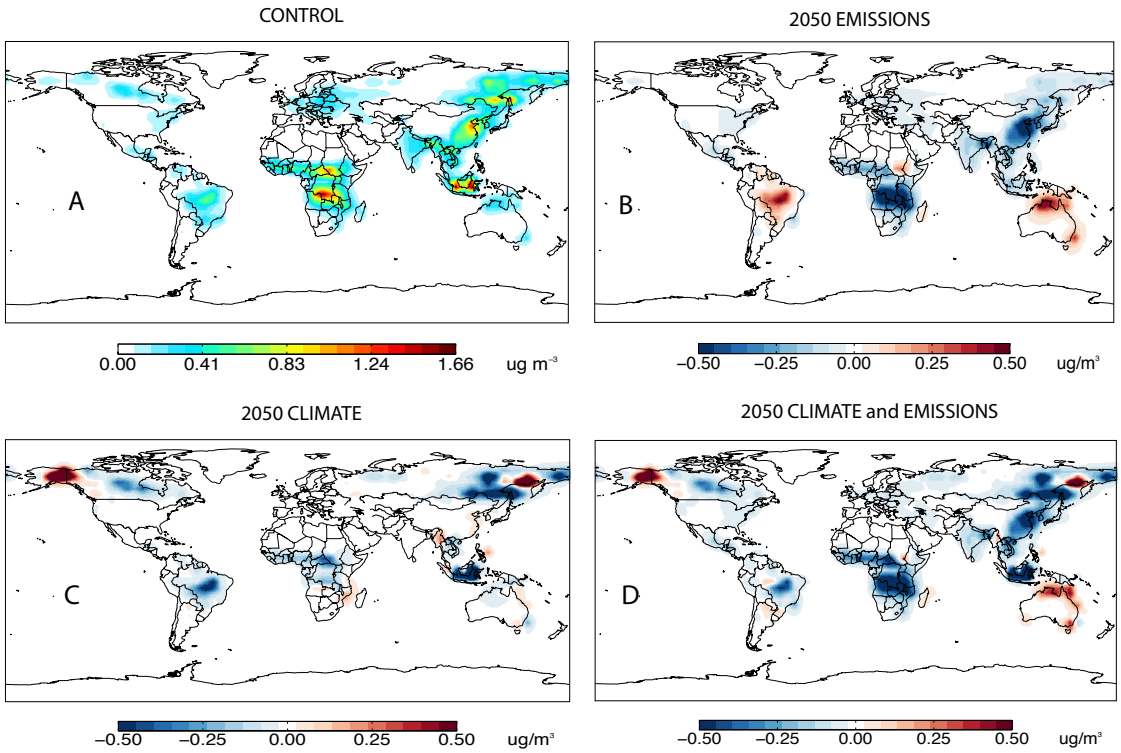

Figure S8. Global concentrations of OC under (A) the control simulation and difference in concentration between the control and simulations under (B) future emissions; (C) future climate, and; (D) future climate and future emissions. Red marks an increase in concentrations, blue marks a decrease.

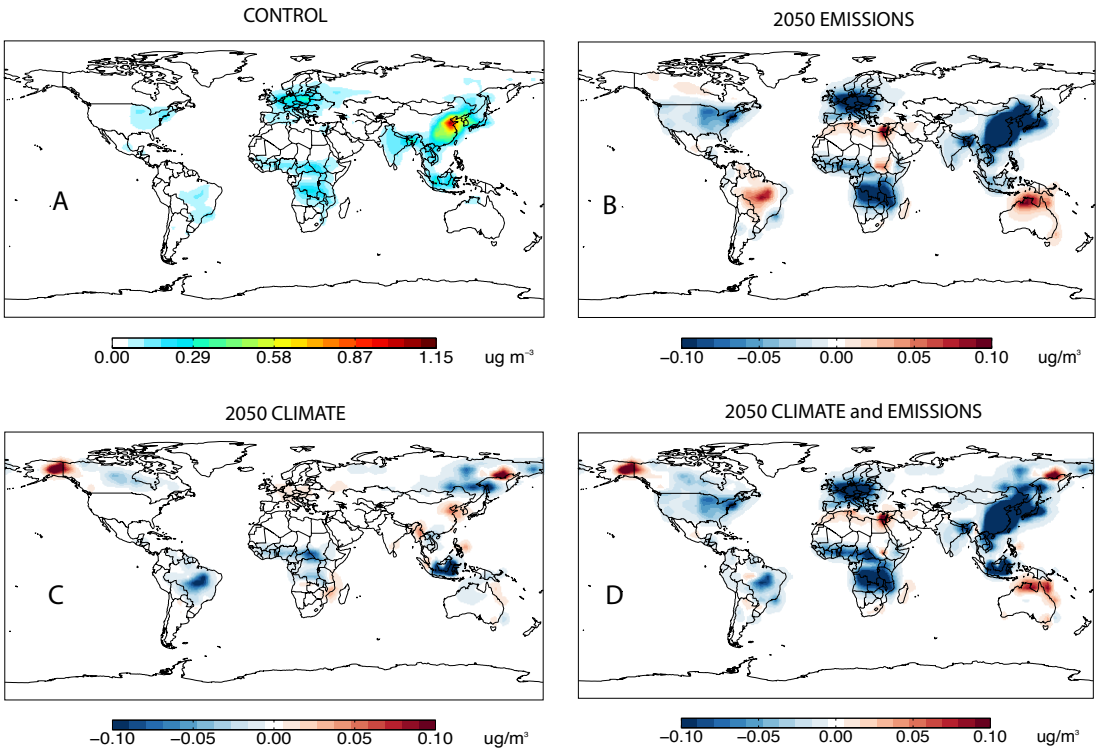

Figure S9. Global concentrations of BC under (A) the control simulation and difference in concentration between the control and simulations under (B) future emissions; (C) future climate, and; (D) future climate and future emissions. Red marks an increase in concentrations, blue marks a decrease.

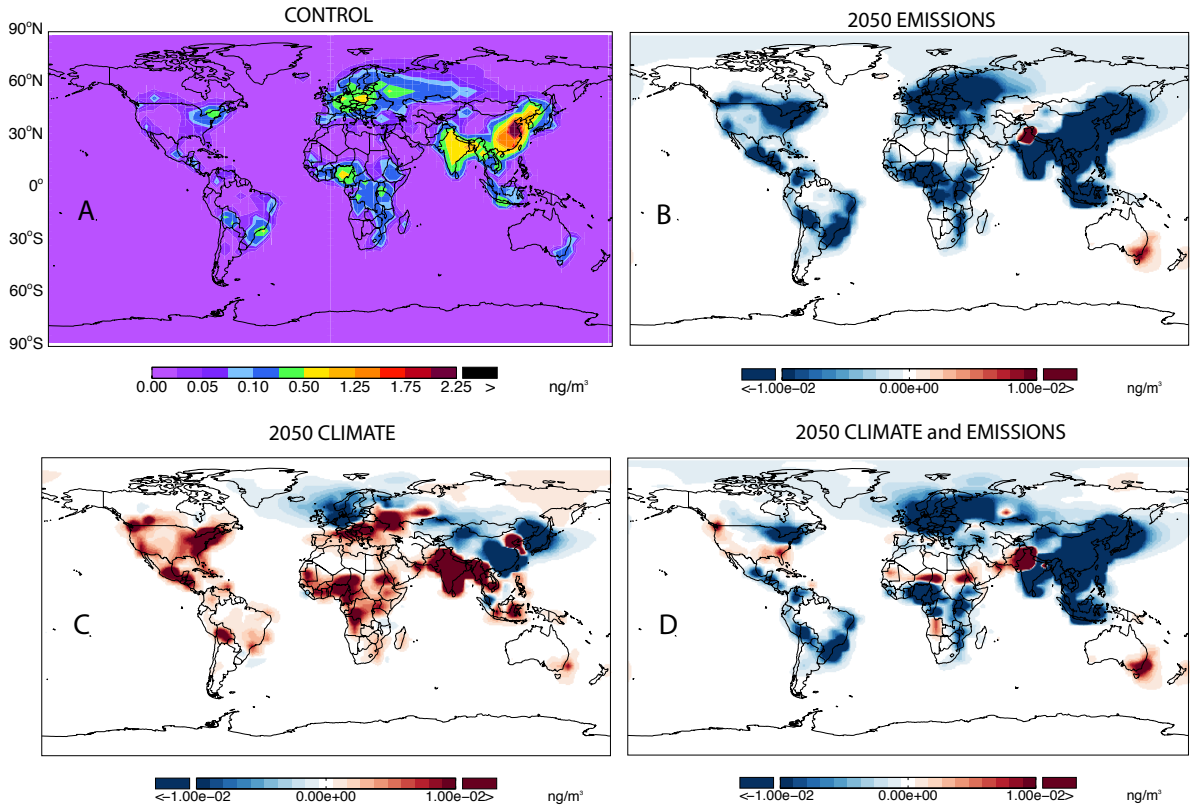

Figure S10. PYR concentrations under (A) the control; concentration differences between the control and simulations under (B) future emissions; (C) future climate; (D) future climate, future emissions. Red marks increases, blue marks decreases.

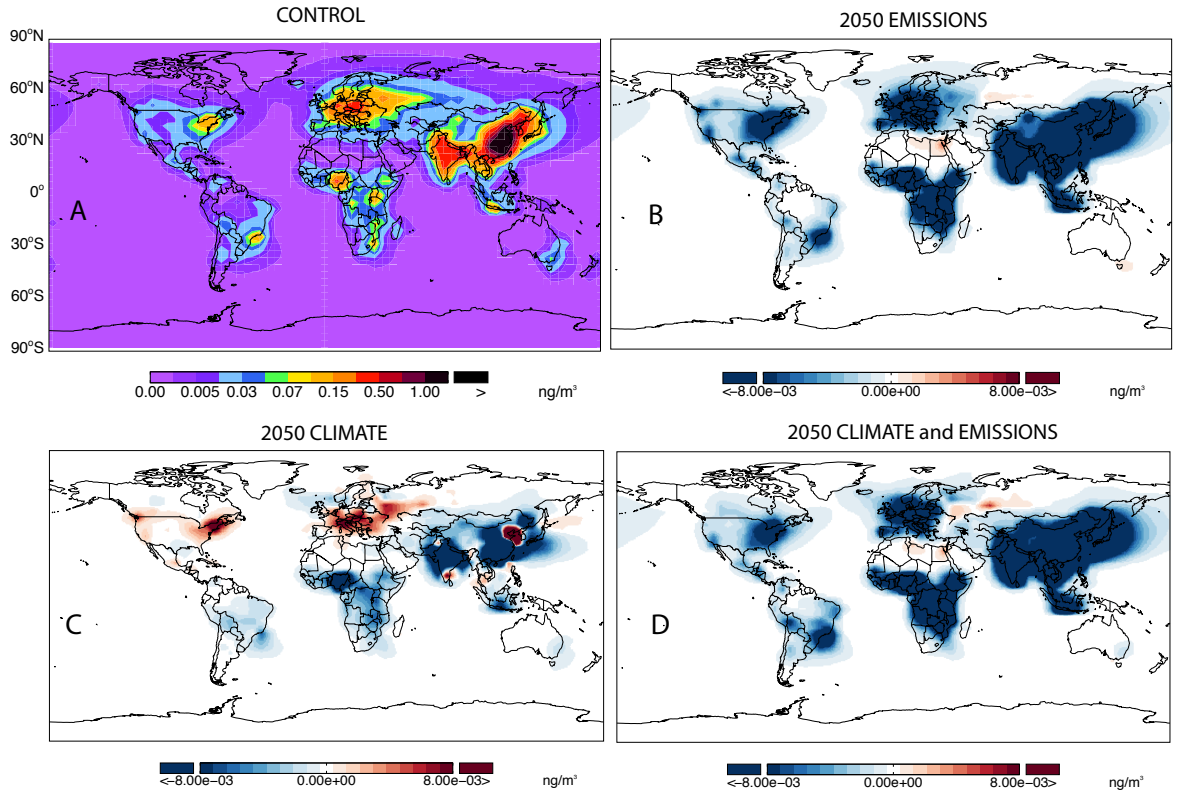

Figure S11. BaP concentrations under (A) the control; concentrations differences between the control and simulations under (B) future emissions; (C) future climate; (D) future climate, future emissions. Red marks increases, blue marks decreases.

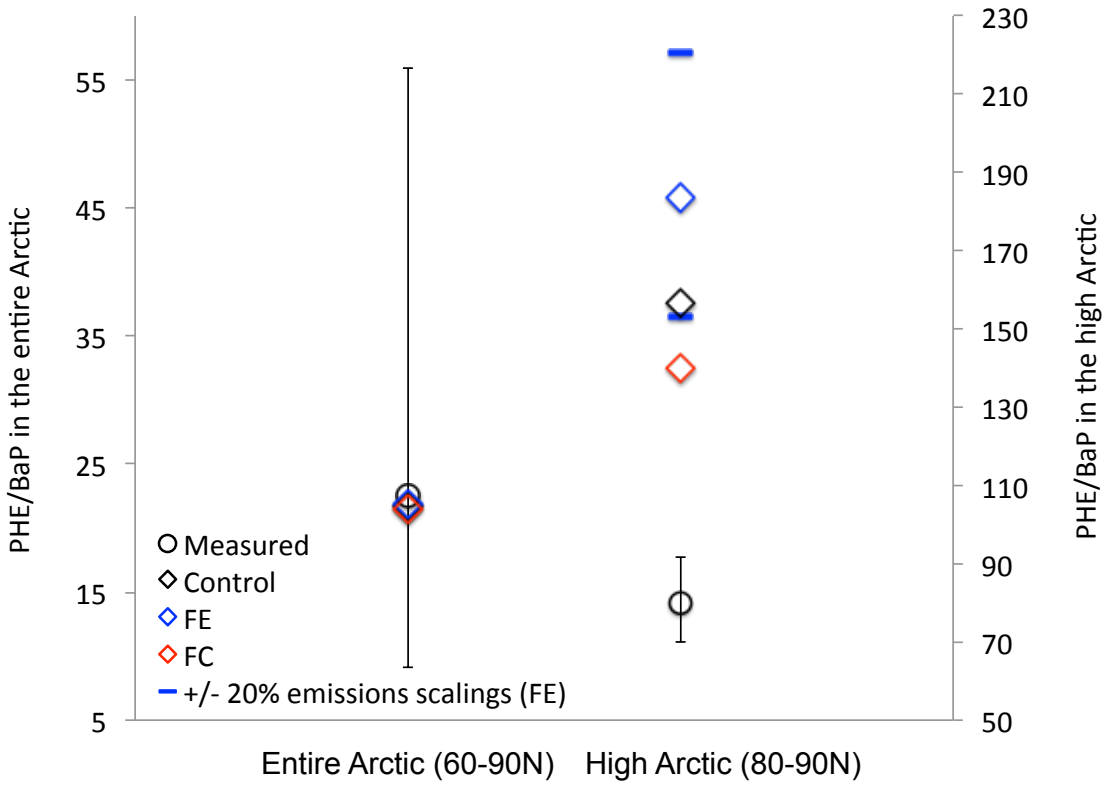

Figure S12. Comparison of simulated mean annual PHE/BaP (control, FE, and FC) to observed in both the entire and high Arctic. Geometric means and standard errors of observed concentrations are from Arctic sites listed in Table 1 of Friedman and Selin[33]. Also shown for the high Arctic is the range of PHE/BaP under FE when anthropogenic emissions are scaled +/-20% of the default projections (blue bars). The relatively large standard error from observations in the entire Arctic forces the symbols representing the means to overlap; the symbol representing the ratio in the control simulation (black diamond) is obscured by the symbols from the FE and FC simulations.

Literature Cited

1. Mackay, D.; Paterson, S. Evaluating the multimedia fate of organic chemics: A level III fugacity model. *Environ. Sci. Technol.* **1991,** *25*, 427-436.

2. Howsam, M.; Jones, K. C.; Ineson, P. Dynamics of PAH deposition, cycling and storage in a mixed- deciduous (Quercus-Fraxinus) woodland ecosystem. *Environ. Poll.* **2001,** *113*, 163-176.

3. Smith-Downey, N.; Sunderland, E.; Jacob, D. Anthropogenic impacts on global storage and emissions of mercury from terrestrial soils: insights from a new global model. *J. Geophys. Res.* **2010,** *115*, G03008.

4. Wang, W.; Simonich, S.; Giri, B.; Chang, Y.; Zhang, Y.; Jia, Y.; Tao, S.; Wang, R.; Wang, B.; Li, W.; Cao, J.; Lu, X. Atmospheric concentrations and air-soil exchange of polycyclic aromatic hydrocarbons (PAHs) in remote, rural village and urban areas of Beijing-Tianjin region, North China. *Sci. Total Environ.* **2011,** *409*, 2942-2950.

5. Cabrerizo, A.; Dachs, J.; Moeckel, C.; Ojeda, M.-J.; Caballero, G.; Barceló, D.; Jones, K. C. Ubiquitous net volatilization of polycyclic aromatic hydrocarbons from soils and parameters influencing their soil-air partition. *Environ. Sci. Technol.* **2011,** *45*, 4740-4747.

6. Liu, G.; Yu, L.; Li, J.; Liu, X.; Zhang, G. PAHs in soils and estimated air-soil exchange in the Pearl River Delta, South China. *Environ. Monit. Assess.* **2011,** *173*, 861-870.

7. Harner, T.; Bidleman, T. F. Octanol-air partition coefficient for describing particle/gas partitioning of aromatic compounds in urban air. *Environ. Sci. Technol.* **1998,** *32*, 1494-1502.

8. Harner, T.; Bidleman, T. F.; Jantunen, L. M. M.; Mackay, D. Soil-air exchange model of persistent pesticides in the United States cotton belt. *Environ. Toxicol. Chem.* **2001,** *20*, 1612-1621.

9. Ribes, S.; Van Drooge, B.; Dachs, J.; Gustafsson, O.; Grimalt, J. O. Influence of soot carbon on the soil-air partitioning of polycyclic aromatic hydrocarbons. *Environ. Sci. Technol.* **2003,** *37*, 2675-2680.

10. Potter, C. S.; Randerson, J. T.; Field, C. B.; Matson, P. A.; Vitousek, P. M.; Mooney, H. A.; Klooster, S. A. Terrestrial ecosystem production: A process model based on global satellite and surface data. *Global Biogeochem. Cycles* **1993,** *7*, 811-841.

11. McLachlan, M. S.; Czub, G.; Wania, F. The influence of vertical sorbed phase transport on the fate of organic chemicals in surface soils. *Environ. Sci. Technol.* **2002,** *36*, 4860-4867.

12. Cousins, I. T.; Mackay, D. Strategies for including vegetation compartments in multimedia models. *Chemosphere* **2001,** *44*, 643-654.

13. Cousins, I. T.; Mackay, D. Transport parameters and mass balance equations for vegetation in Level III fugacity models. Internal report published on the website of the Canadian Environmental Modelling Centre (http://www.trent.ca/envmodel/). **2000**.

14. Simonich, S. L.; Hites, R. A. Vegetation-atmosphere partitioning of polycyclic aromatic hydrocarbons. *Environ. Sci. Technol.* **1994,** *28*, 939-943.

15. Tremolada, P.; Burnett, V.; Calamari, D.; Jones, K. C. Spatial distribution of PAHs in the UK atmosphere using pine needles. *Environ. Sci. Technol.* **1996,** *30*, 3570-3577.

16. Ma, Y.-G.; Lei, Y.; Xiao, H.; Wania, F.; Wang, W.-H. Critical review and recommended values for the physical-chemical property data of 15 polycyclic aromatic hydrocarbons at 25 °C. *J. Chem. Eng. Data* **2010,** *55*, 819-825.

17. Lohmann, R.; Lammel, G. Adsorptive and absorptive contributions to the gas-particle partitioning of polycyclic aromatic hydrocarbons: State of knowledge and recommended parametrization for modeling. *Environ. Sci. Technol.* **2004,** *38*, 3793-3803.

18. Schwarzenbach, R. P.; Gschwend, P. M.; Imboden, D. M., *Environmental Organic Chemistry*. 2nd ed.; 2003.

19. Brubaker, W. W.; Hites, R. A. OH reaction kinetics of polycyclic aromatic hydrocarbons and polychlorinated dibenzo-p-dioxins and dibenzofurans. *J. Phys. Chem. A* **1998,** *102*, 915-921.

20. EPA, U. S. Estimation Programs Interface Suite for Microsoft Windows, v 4.10. United States Environmental Protection Agency, Washington DC, USA. **2011**.

21. Kahan, T. F.; Kwamena, N.-O. A.; Donaldson, D. J. Heterogeneous ozonation kinetics of polycyclic aromatic hydrocarbons on organic films. *Atmos. Environ.* **2006,** *40*, 3448-3459.

22. Park, R. J.; Jacob, D. J.; Chin, M.; Martin, R. V. Sources of carbonaceous aerosols over the United States and implications for natural visibility. *J. Geophys. Res.* **2003,** *108(D12)*, 4355.

23. IMAGE. The Image 2.2 implementatino of the SRES scenarios, *Publ. 481508018*, [CD-ROM], Natl. Inst. for Public Health and the Environ., Bilthoven, Netherlands, July. **2001**.

24. Wu, S.; Mickley, L. J.; Jacob, D. J.; Rind, D.; Streets, D. G. Effects of 2000-2050 changes in climate and emissions on global tropospheric ozone and the policy-relevant background surface ozone in the United States. *J. Geophys. Res.* **2008,** *113*, D18312.

25. Streets, D. G.; Bond, T. C.; Lee, T.; Jang, C. On the future of carbonaceous aerosol emissions. *J. Geophys. Res.* **2004,** *109*, D24212.

26. Pye, H. O. T.; Liao, H.; Wu, S.; Mickley, L. J.; Jacob, D. J.; Henze, D. K.; Seinfeld, J. H. Effect of changes in climate and emissions on future sulfate-nitrate-ammonium aerosol levels in the United States. *J. Geophys. Res.* **2009,** *114*, D01205.

27. Wu, S.; Mickley, L. J.; Leibensperger, E. M.; Jacob, D. J.; Rind, D.; Streets, D. G. Effects of 2000-2050 global change on ozone air quality in the United States. *J. Geophys. Res.* **2008,** *113*, D06302.

28. Knorr, W.; Lehsten, V.; Arneth, A. Determinants and predictability of global wildfire emissions. *Atmos. Chem. Phys.* **2012,** *12*, 6845-6861.

29. Beyer, A.; Wania, F.; Gouin, T.; Mackay, D.; Matthies, M. Selecting internally consistent physicochemical properties of organic compounds. *Environ. Toxicol. Chem.* **2002,** *21*, 941-953.

30. Odabasi, M.; Cetin, E.; Sofuoglu, A. Determination of octanol-air partition coefficients and supercooled liquid vapor pressures of PAHs as a function of temperature: Application to gas-particle partitioning in an urban atmosphere. *Atmos. Environ.* **2006,** *40*, 6615-6625.

31. Shiu, W.-Y.; Ma, K.-C. Temperature dependence of physical-chemical properties of selected chemicals of environmental interest. I. Mononuclear and polynuclear aromatic hydrocarbons. *J. Phys. Chem. Ref. Data* **2000,** *29*, 41-130.

32. Biermann, H. W.; Mac Leod, H.; Atkinson, R.; Winer, A. M.; Pitts, J. N. Kinetics of the gas-phase reactions of the hydroxyl radical with naphthalene, phenanthrene, and anthracene. *Environ. Sci. Technol.* **1985,** *19*, 244-248.

33. Friedman, C. L.; Selin, N. E. Long-range atmospheric transport of polycyclic aromatic hydrocarbons: A global 3-D model analysis including evaluation of Arctic sources. *Environ. Sci. Technol.* **2012,** *46*, 9501-9510.

34. Peters, G. P.; Nilssen, T. B.; Lindholt, L.; Eide, M. S.; Glomsrød, S.; Eide, L. I.; Fuglestvedt, J. S. Future emissions from shipping and petroleum activities in the Arctic. *Atmos. Chem. Phys.* **2011,** *11*, 5305-5320.